

Metric from Human: Zero-shot Monocular Metric Depth Estimation via Test-time Adaptation

Yizhou Zhao¹, Hengwei Bian¹, Kaihua Chen¹, Pengliang Ji¹, Liao Qu¹, Shao-yu Lin¹,
Weichen Yu¹, Haoran Li², Hao Chen¹, Jun Shen², Bhiksha Raj¹, Min Xu^{1*}

¹Carnegie Mellon University, Pittsburgh ²University of Wollongong, Wollongong

<https://github.com/Skaldak/MfH>

Abstract

Monocular depth estimation (MDE) is fundamental for deriving 3D scene structures from 2D images. While state-of-the-art monocular relative depth estimation (MRDE) excels in estimating relative depths for in-the-wild images, current monocular metric depth estimation (MMDE) approaches still face challenges in handling unseen scenes. Since MMDE can be viewed as the composition of MRDE and metric scale recovery, we attribute this difficulty to scene dependency, where MMDE models rely on scenes observed during supervised training for predicting scene scales during inference. To address this issue, we propose to use humans as landmarks for distilling scene-independent metric scale priors from generative painting models. Our approach, Metric from Human (MfH), bridges from generalizable MRDE to zero-shot MMDE in a generate-and-estimate manner. Specifically, MfH generates humans on the input image with generative painting and estimates human dimensions with an off-the-shelf human mesh recovery (HMR) model. Based on MRDE predictions, it propagates the metric information from painted humans to the contexts, resulting in metric depth estimations for the original input. Through this annotation-free test-time adaptation, MfH achieves superior zero-shot performance in MMDE, demonstrating its strong generalization ability.

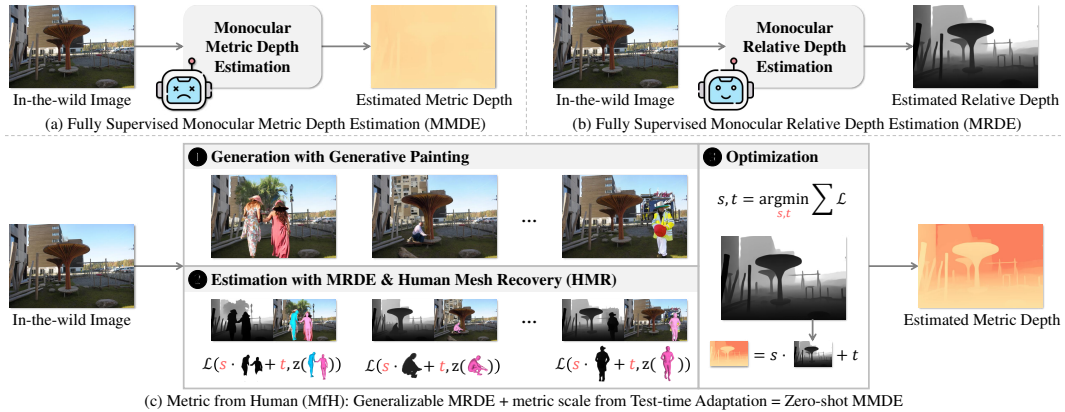


Figure 1: **Illustration of our motivation.** (a) Fully supervised MMDE cannot generalize well on unseen data as (b) MRDE, with its reliance on training scenes for predicting metric scales during test time. (c) Hence, we develop MfH to distill metric scale priors from generative models in a generate-and-estimate manner, bridging the gap from generalizable MRDE to zero-shot MMDE. We use grayscale to represent normalized depths in MRDE predictions, while a colormap mapping metric depth from meters to RGB values in MMDE results. In ②, $z(\cdot)$ denotes rasterized metric depths.

*Corresponding author.

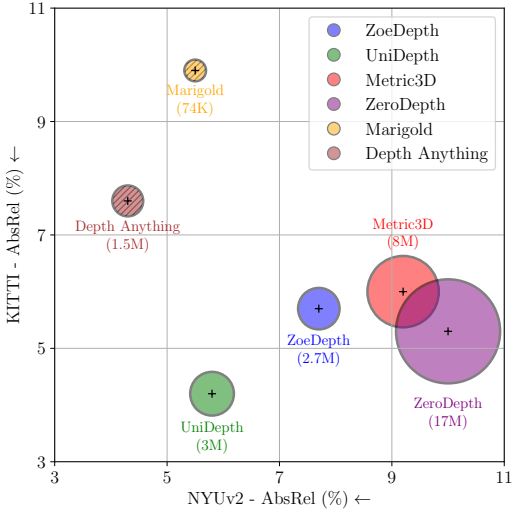


Figure 2: **Comparison of state-of-the-art MRDE and MMDE methods in terms of AbsRel and the number of training samples.** Marigold [1] and Depth Anything [2] are designed for MRDE, while the rest are for MMDE. We observe MMDE approaches require notably more data to achieve similar AbsRel as MRDE.

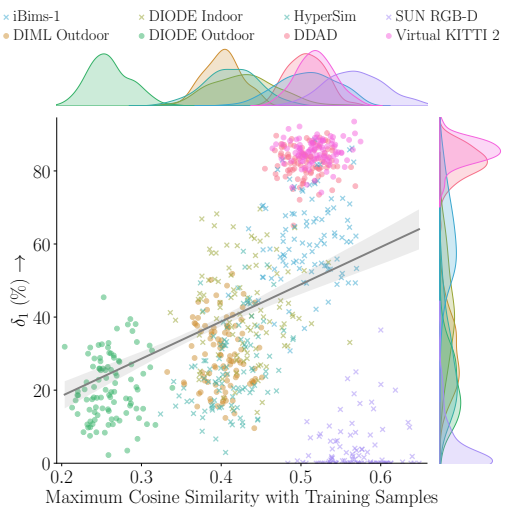


Figure 3: **MMDE δ_1 versus the maximum cosine similarity between each test sample and all metric-annotated training samples.** “ \times/\circ ”: from indoor/outdoor datasets. We see that the scale-related performance of a test sample positively correlates with its similarity to training samples. Details can be found in Appendix A.1.

1 Introduction

Monocular depth estimation (MDE) is essential in understanding the 3D structure of scenes from 2D images and has many applications in robotics [3, 4], autonomous driving [5, 6], and virtual reality [7, 8]. It requires recovering depth information from a single image without relying on additional sensors or stereo cameras, thereby being inherently ill-posed.

Recent literature mainly explores MDE in two branches, namely, monocular relative depth estimation (MRDE) [2, 1, 9] and monocular metric depth estimation (MMDE) [10–17]. MRDE estimates normalized depths or disparities by factoring out the scale. Its scale-invariant nature enables large-scale training on diverse datasets with distinct camera parameters, while at the cost of bringing in scale ambiguity. In contrast, MMDE predicts absolute depths in *meters*. Due to the unbounded output range and the intertwined relationship between depths and focal lengths, early works of this line often cannot perform well on test data with arbitrary scene scales or camera intrinsics. To compensate for this, recent progress resorts to injecting scene information [12] or camera information [10, 11, 14] into the model. The former attempt learns scene-specific scale priors, modeled with metric heads for indoor or outdoor scenes, and uses either to transform relative depths into metric depths in a heuristic manner. The latter aims to disambiguate scale prediction with extra camera inputs. However, as shown in Fig. 2, both lines of work require notably larger amounts of labeled training data to achieve similar mean absolute relative errors (AbsRel) as their MRDE counterparts.

What causes the data hunger of MMDE, and what makes MMDE harder to generalize? Given that MMDE can be viewed as the composition of MRDE and metric scale recovery, we posit the latter might be the primary factor. MMDE models might face challenges in inferring scene scales without sufficient exposure to similar annotated scenes during training, which is not a problem for scale-invariant MRDE. To validate our assumption, we evaluate a scale-related metric (δ_1) of an MMDE model, ZoeDepth [12], on randomly sampled test images. Meanwhile, we calculate the maximum cosine similarity between each test sample and all training samples with metric annotations using DINOv2 [18]. Our findings from Fig. 3 indicate a clear trend: higher similarity to training samples positively correlates with better performance, and vice versa. This reflects a scene dependency of MMDE models, likely arising from their supervised training paradigm. In other words, they tend to learn an implicit mapping between training scenes and metric scales from \langle image, metric annotation \rangle pairs. As a result, adapting to novel scenes may require extra domain-specific fine-tuning.

To address this dependency for better generalization capabilities, we propose to avoid scene-dependent supervised learning, while leveraging a scene-independent metric scale prior. Our insights are two-fold. First, we observe generative painting models can paint objects of proper sizes based on partial contexts, indicating an underlying sense of scales. Additionally, humans can be potentially utilized as relatively universal landmarks, since humans exhibit sizes that are generally more comparable to each other than other common in-the-wild objects, e.g., tables, trees, and cars. To explicitly derive a metric scale prior from generative painting models, we notice state-of-the-art human mesh recovery (HMR) approaches [19–21] can robustly estimate human dimensions for in-the-wild images. Also, they typically output SMPL [22, 23] representations with shape space defined in *meters*. While the input image does not guarantee to include humans, we speculate an off-the-shelf image painting model can paint proportionate humans in the scene, which provides an opportunity to retrieve metric-scale information for the original input by measuring painted humans. Hence, we introduce a test-time adaptation pipeline, Metric from Human (MfH), as illustrated in Fig. 1. Concretely, it 1) paints humans with partial contexts of the input image, 2) estimates human dimensions from the painted image, and 3) propagates the metric-scale information from humans to the contexts for MMDE. In this way, we can distill the metric scale prior hidden inside the generative painting model, unleashing its power to comprehend diverse scenes. As a result, our MfH mitigates the scene dependency issue in fully supervised MMDE, thereby being potentially more generalizable to unseen scenes.

Our contributions can be summed up as follows:

1. We discuss that the current obstacle for generalizable MMDE lies in scene dependency and propose to use a scene-independent metric scale prior as a solution. Further, we find it possible to establish such prior by distilling from generative painting models.
2. To extract the metric scale prior from generative painting models for zero-shot MMDE, we design a test-time adaptation framework, Metric from Human (MfH). Using humans as landmarks, we bridge from MRDE to MMDE by a generate-and-estimate pipeline.
3. Through qualitative and quantitative experiments, we demonstrate the superiority and generalization ability of our MfH in zero-shot MMDE, needless of any metric depth annotations.

2 Related Work

Monocular Depth Estimation (MDE) has garnered significant interest in recent years. Early approaches focused on supervised methods that predict either monocular metric depth estimation (MMDE) [16, 24–27, 15] or monocular relative depth estimation (MRDE) [27–29, 9]. Despite remarkable progress in network architectures [30–33, 16, 13, 34, 15], existing MMDE methods often confine their training and testing to specific domains, leading to performance degradation under minor domain shifts and poor generalization to unseen environments. In contrast, relative depth models have demonstrated better generalization by leveraging scale-invariant losses [9, 35, 36] on diverse datasets. However, these models cannot recover metric scales, which are crucial for downstream applications. Recent works explored generalizable MMDE models [12, 11, 14, 10] for diverse domains, leveraging camera awareness through explicit incorporation of intrinsics [37, 11] or normalization based on camera properties [38, 17, 14]. They often require fine-tuning to adjust to specific domains [11, 10]. Several recent studies explore zero-shot MMDE, using language as a prior to ground predictions to metric scale [39–41]. However, their hand-crafted depth captions to connect the language and metric worlds are often too coarse to capture accurate depths. Our MfH instead distills metric scale priors from generative painting models, enhancing both the generalization capability and pixel-wise precision of zero-shot MMDE models without relying on metric depth annotations.

Human Mesh Recovery (HMR) aims to reconstruct 3D human bodies from visual inputs. Optimization-based HMR relies on iterative optimization techniques to fit parametric body models such as SMPL to detect image features. Examples include SMPLify [42] and its variants [23, 43], which iteratively minimize an objective function to align the model with 2D key points and silhouettes. In contrast, feed-forward methods [44–49] directly regress the body shape and pose parameters from a single image using deep learning techniques. Among them, HMR 2.0 [20] is a fully transformer-based approach for recovering 3D human meshes from single images. We adopt it as our HMR model for estimating in-the-wild human structures and poses. With HMR, we derive metric scale priors from generative painting models, thereby bridging generalizable MRDE to zero-shot MMDE.

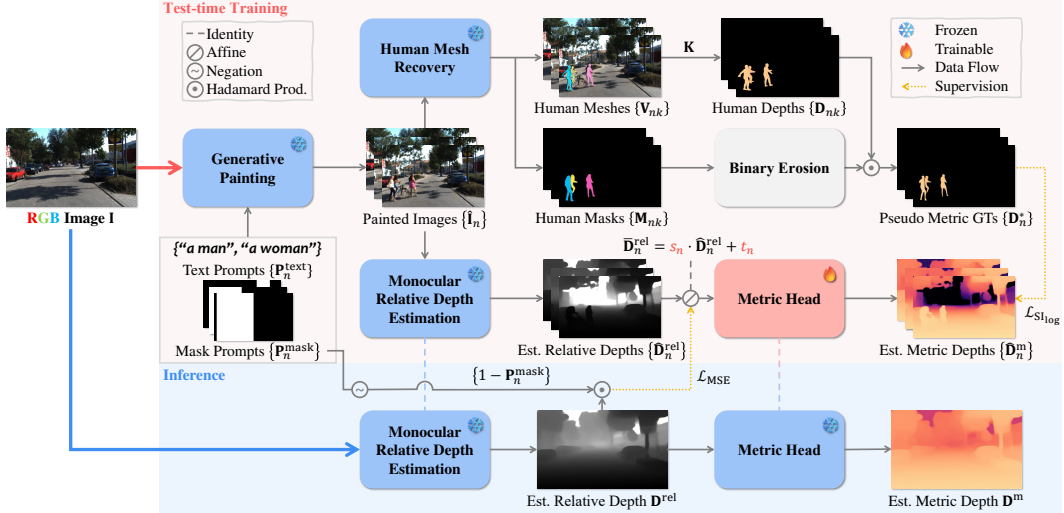


Figure 4: **The framework of Metric from Human (MfH).** Our pipeline comprises two phases. The test-time training phase learns a metric head that transforms relative depths into metric depths based on images randomly painted upon the input image and the corresponding pseudo ground truths. After training the metric head, the inference phase estimates metric depths for the original input.

3 Method

Taking an RGB image $\mathbf{I} \in \mathbb{R}^{H \times W \times 3}$ with its camera intrinsic $\mathbf{K} \in \mathbb{R}^{3 \times 3}$ as input, we aim to estimate its pixel-wise metric depths $\mathbf{D}^m \in \mathbb{R}^{H \times W \times 1}$. Unlike existing MMDE methods [12, 11, 14, 10] that typically train on images with metric annotations and expect the trained model to generalize to unseen inputs, we instead consider a test-time adaptation scenario. That is, to estimate metric depths on a certain image without training on domain-specific metric annotations. To achieve this, we propose a framework to learn a metric head for each input \mathbf{I} , as depicted in Fig. 4. The metric head is concatenated after an off-the-shelf MRDE model to transform relative depths into metric depths. While the inference pipeline is simplistic, our key insight is to use humans as metric landmarks during test-time training. Since humans are not guaranteed to exist in in-the-wild images, we introduce a generate-and-estimate method in Sec. 3.2 to extract metric scale information from the given image. This extracted information together with the estimated relative depths allows us to approach annotation-free zero-shot metric depth estimation, as outlined in Sec. 3.3.

3.1 Preliminaries

3.1.1 Monocular Depth Estimation (MDE)

Assuming a pinhole camera model, we have the following relation

$$\mathbf{D}^m = \frac{b \cdot f}{\mathbf{d}^m}, \quad \mathbf{D}^{\text{rel}} = \text{rel}(\mathbf{D}^m) = \frac{\mathbf{D}^m - t(\mathbf{D}^m)}{s(\mathbf{D}^m)}, \quad (1)$$

where b and f are the camera baseline and focal length, \mathbf{D}^m and \mathbf{d}^m are metric depths and disparities, and $s(\cdot)$ and $t(\cdot)$ are scalar functions, denoting a scale and a translation to normalize the input. We use superscript m and rel to refer to metric and relative values, accordingly. Due to the correlation between camera parameters and the scale of depth, MMDE cannot generalize well if the camera intrinsic is unknown or the scene scale is hard to predict, e.g., when the scene is unseen during training. In contrast, MRDE enjoys better generalization ability for its affine-invariant formulation.

3.1.2 Human Mesh Recovery (HMR)

We adopt a state-of-the-art HMR model, HMR 2.0 [20], for reconstructing camera-frame human meshes from an image $\hat{\mathbf{I}}_n \in \mathbb{R}^{H \times W \times 3}$ with K people. Starting with human segmentation masks $\{\mathbf{M}_{nk} \in \mathbb{R}^{H \times W \times 1}\}_{k=1}^K$ from Mask R-CNN [50], HMR 2.0 predicts SMPL [22] parameters for each

human as $\{\Phi_{nk}, \theta_{nk}, \beta_{nk}, \Gamma_{nk}\}_{k=1}^K$. These parameters represent global orientation $\Phi_{nk} \in \mathbb{R}^{3 \times 3}$, body pose $\theta_{nk} \in \mathbb{R}^{22 \times 3 \times 3}$, shape $\beta_{nk} \in \mathbb{R}^{10}$, and root translation $\Gamma_{nk} \in \mathbb{R}^3$. Then the human body meshes with vertices $\mathbf{V}_{nk} \in \mathbb{R}^{3 \times 6890}$ can be recovered with the SMPL model

$$\mathbf{V}_{nk} = \text{SMPL}(\Phi_{nk}, \theta_{nk}, \beta_{nk}) + \Gamma_{nk}, \text{ where } k = 1, 2, \dots, K. \quad (2)$$

Since the shape space of SMPL is defined in *meters*, the generated vertices $\{\mathbf{V}_{nk}\}$ are also in *meters*. As a result, all HMR regressors, such as HMR 2.0 we use, inherit such data prior.

3.2 Generating Humans as Metric Landmarks

To start off, we randomly place people on the input image with generative image painting, with text prompts $\{\mathbf{P}_n^{\text{text}}\}_{n=1}^N$ sampled from {"a man", "a woman"} and mask prompts $\{\mathbf{P}_n^{\text{mask}} \in \mathbb{R}^{H \times W \times 1}\}_{n=1}^N$ sampled from rectangles smaller than the whole image. We write $\mathbf{P}_n = (\mathbf{P}_n^{\text{text}}, \mathbf{P}_n^{\text{mask}})$ as a shorthand. Once at a time, we randomly generate N painted images with humans

$$\hat{\mathbf{I}}_n = \text{paint}(\mathbf{I} | \mathbf{P}_n), \text{ where } n = 1, 2, \dots, N, \quad (3)$$

and $\{\hat{\mathbf{I}}_n \in \mathbb{R}^{H \times W \times 3}\}_{n=1}^N$ are the painted images. We observe the generative image painting model can paint people of proper sizes that are compatible with the unmasked background. This allows us to use the painted people as landmarks to inform our model of the metric scale. To this end, we fed these painted images into HMR 2.0 to predict human instance segmentation masks $\{\mathbf{M}_{nk}\}_{n=1, k=1}^{N, K}$ and meshes $\{\mathbf{V}_{nk}\}_{n=1, k=1}^{N, K}$, where the subscripts denote the k -th person in the n -th image. We obtain the pseudo metric ground truths \mathbf{D}_n^* with rasterization

$$\mathbf{D}_n^* = \min_k [\text{erode}(\mathbf{M}_{nk} \cap \mathbf{S}_{nk}) \odot \mathbf{D}_{nk}], \quad (4)$$

where $\mathbf{S}_{nk}, \mathbf{D}_{nk} = \rho(\mathbf{K}, \mathbf{V}_{nk})$ are the rasterized silhouettes and depths, respectively, and \odot stands for the Hadamard product. We erode the intersection of the instance segmentation mask \mathbf{M}_{nk} and the rasterized silhouette \mathbf{S}_{nk} to avoid overlapping and take the minimum of k depth maps so that the depth values from closer humans can occlude the farther ones. Using these pseudo ground truths, we supervise the learning of the metric head with the scale-invariant log (SI_{log}) loss [51]

$$\mathcal{L}_{\text{SI}_{\log}}(\hat{\mathbf{D}}_n^m, \mathbf{D}_n^*) = \frac{1}{HW} \sum_i \epsilon_i^2 - \frac{\lambda}{(HW)^2} \left(\sum_i \epsilon_i \right)^2, \quad (5)$$

where $\epsilon = \log \hat{\mathbf{D}}_n^m - \log \mathbf{D}_n^*$, with $\hat{\mathbf{D}}_n^m$ being the estimated metric depth map, subscript i denotes the index of each pixel, and $\lambda \in [0, 1]$. Since the rasterized depths \mathbf{D}_{nk} are in *meters* and the first term in $\mathcal{L}_{\text{SI}_{\log}}$ is pixel-wise l_2 , this loss provides crucial metric scale information to the metric head.

3.3 Transforming Relative Depths into Metric Depths

During training, we estimate a relative depth map $\hat{\mathbf{D}}_n^{\text{rel}}$ for each painted image $\hat{\mathbf{I}}_n$ with a pre-trained MRDE model, and learn a metric head to transform $\hat{\mathbf{D}}_n^{\text{rel}}$ into an estimated metric depth map $\hat{\mathbf{D}}_n^m$. Similarly, we obtain \mathbf{D}^{rel} and \mathbf{D}^m from the original input \mathbf{I} during inference. According to Eq. (1), we can learn a simple linear layer as our metric head, i.e., $\hat{\mathbf{D}}_n^m = \hat{s} \cdot \hat{\mathbf{D}}_n^{\text{rel}} + \hat{t}$. In addition, we need to account for the difference between the relative depths predicted from the original image \mathbf{D}^{rel} and those from the painted images $\{\hat{\mathbf{D}}_n^{\text{rel}}\}$ on the unpainted regions. Considering the affine-invariant nature of MRDE, we further decompose metric depth predictions with

$$\hat{\mathbf{D}}_n^m = s \cdot (s_n \cdot \hat{\mathbf{D}}_n^{\text{rel}} + t_n) + t = s \cdot \bar{\mathbf{D}}_n^{\text{rel}} + t, \text{ where } \bar{\mathbf{D}}_n^{\text{rel}} = s_n \cdot \hat{\mathbf{D}}_n^{\text{rel}} + t_n, \quad (6)$$

and $\{s_n\}, \{t_n\}, s, t \in \mathbb{R}$ are optimizable parameters. Then we align \mathbf{D}^{rel} and $\{\hat{\mathbf{D}}_n^{\text{rel}}\}$ with

$$\mathcal{L}_{\text{MSE}}(\bar{\mathbf{D}}_n^{\text{rel}}, \mathbf{D}^{\text{rel}}) = \left\| (1 - \mathbf{P}_n^{\text{mask}}) \odot (\bar{\mathbf{D}}_n^{\text{rel}} - \mathbf{D}^{\text{rel}}) \right\|_2. \quad (7)$$

This objective considers the pixel-wise alignment of unpainted regions with an affine transform specific to each painted image. Finally, we formulate our complete objective function as

$$\min_{s, t} \sum_n \mathcal{L}_{\text{SI}_{\log}}(\hat{\mathbf{D}}_n^m, \mathbf{D}_n^*) + \sum_n \min_{s_n, t_n} \mathcal{L}_{\text{MSE}}(\bar{\mathbf{D}}_n^{\text{rel}}, \mathbf{D}^{\text{rel}}). \quad (8)$$

Table 1: Performance comparisons of our MfH and state-of-the-art methods on the NYU-Depth V2 [52] and KITTI [55] datasets. [†]LORN uses 200 images and 2,500 partial images for training.

Method	Supervision	NYUv2				KITTI			
		$\delta_1 \uparrow$	AbsRel \downarrow	SI _{log} \downarrow	RMSE \downarrow	$\delta_1 \uparrow$	AbsRel \downarrow	SI _{log} \downarrow	RMSE \downarrow
ZeroDepth [11]	many-shot	90.1	10.0	—	0.380	89.2	10.2	—	4.38
Metric3D [14]	many-shot	92.6	9.38	9.13	0.337	97.5	5.33	7.28	2.26
UniDepth-C [10]	many-shot	97.2	6.26	6.41	0.232	97.9	4.69	6.71	2.00
UniDepth-V [10]	many-shot	98.4	5.78	5.27	0.201	98.6	4.21	5.84	1.75
LORN [58] [†]	few-shot	70.3	101	—	9.452	—	—	—	—
Hu et al. [40]	one-shot	42.8	34.7	—	1.049	31.2	38.4	—	12.29
DepthCLIP [59]	zero-shot	39.4	38.8	—	1.167	28.1	47.3	—	12.96
MfH (Ours)	zero-shot	83.2	13.7	9.78	0.487	81.2	13.3	10.5	4.21

Such formulation propagates metric scale information from human pixels to background pixels, thereby enabling the metric head to predict for the non-human context. After optimization, it is then possible to infer metric depths for the original input image. While one can deploy fancier metric head and apply up-to-affine consistency constraints between aligned relative depth predictions \bar{D}_n^{rel} and metric depth predictions \hat{D}_n^{m} for better robustness, we observe a simple affine transform is capable of providing good predictions, leaving further parameterization for future works.

4 Experiments

4.1 Experimental Setting

Datasets. Under our test-time adaptation setting, we do not train on any datasets but only test on each input image directly after image-specific optimizations. Specifically, we evaluate the zero-shot MMDE capability of MfH on NYU-Depth V2 [52], IBims-1 [53], ETH-3D [54] with the split from [13] and official masks, and KITTI [55] with the corrected Eigen-split from [51]. Following prior works [12, 15, 16], we apply the Eigen evaluation mask [51] on NYU-Depth V2 and IBims-1 while the Garg evaluation mask [56] on KITTI.

Evaluation Metrics. We employ several common metrics to assess the performance of all baseline methods and our model. The $\delta_1 = \frac{1}{HW} \sum_{i=1}^{HW} \left[\max \left(\frac{D_{\text{pred}}}{D_{\text{gt}}}, \frac{D_{\text{gt}}}{D_{\text{pred}}} \right) < 1.25 \right]$ metric evaluates the fraction of predicted depth values that are within a threshold factor of their corresponding true values; the Mean Absolute Relative Error, $\text{AbsRel} = \frac{1}{HW} \sum_{i=1}^{HW} \frac{|D_{\text{gt}} - D_{\text{pred}}|}{D_{\text{gt}}}$, measures the average absolute difference between the predicted and true depth values, normalized by the true depth; the Scale Invariant Logarithmic Error, $\text{SI}_{\log} = 100 \sqrt{\text{Var}(\log D_{\text{pred}} - \log D_{\text{gt}})}$, quantifies the error in a logarithmic scale that is invariant to the absolute scale of the scene; the Root Mean Squared Error, $\text{RMSE} = \sqrt{\frac{1}{HW} \sum_{i=1}^{HW} (D_{\text{gt}} - D_{\text{pred}})^2}$, focuses on the square root of the mean of squared differences between the predicted and actual depth values, emphasizing larger errors.

Implementation Details. We adopt Depth Anything [2] without fintuning on metric annotations as our MRDE model, Stable Diffusion v2 [57] for generative painting, and HMR 2.0 [20] for human mesh recovery. In $\mathcal{L}_{\text{SI}_{\log}}$, we follow ZoeDepth [12] to set the $\lambda = 0.15$. For optimizing the alignment parameters $\{s_n\}, \{t_n\}$, we leverage linear regression to obtain a close-formed solution. As for optimizing the metric head parameters, s, t , we use the L-BFGS optimizer with a fixed learning rate of 1 for 50 steps. Unless otherwise specified, we randomly paint 32 images for our comparison experiments and 4 for our ablation studies. All experiments are run on one NVIDIA A100 GPU.

4.2 Comparison Results

We first evaluate the MMDE results on NYU-Depth V2 [52] and KITTI [55], common benchmarks with indoor and outdoor scenes, respectively. In Tab. 1, we show that our zero-shot MfH consistently outperforms other approaches trained with few/one/zero-shot supervision. This indicates that generative painting models are capable of capturing metric scale information, which is potentially more accurate than that embedded in language models [40, 59]. With our generate-and-estimate pipeline, the metric scale prior hidden inside generative painting models can be leveraged for zero-shot MMDE.

Table 2: Performance comparisons of our MfH and many-shot methods on the DIODE (Indoor) [60], iBims-1 [61], and ETH3D [54] datasets. *-{N, K, NK}: fine-tuned on NYUv2 [52], KITTI [55], or the union of them. We re-evaluate all results with a consistent pipeline for metric completeness.

Method	DIODE (Indoor)				iBims-1				ETH3D			
	$\delta_1 \uparrow$	AbsRel \downarrow	SI _{log} \downarrow	RMSE \downarrow	$\delta_1 \uparrow$	AbsRel \downarrow	SI _{log} \downarrow	RMSE \downarrow	$\delta_1 \uparrow$	AbsRel \downarrow	SI _{log} \downarrow	RMSE \downarrow
ZoeDepth-NK [12]	38.8	33.0	13.3	1.598	61.0	18.7	8.98	0.778	33.5	47.3	14.0	2.094
Depth Anything-N [2]	29.7	32.7	12.5	1.486	71.3	15.0	7.58	0.594	25.2	38.7	10.2	2.327
Depth Anything-K [2]	11.1	231	15.5	5.199	2.88	217	17.2	5.385	16.9	136	17.1	4.202
ZeroDepth [11]	43.2	30.0	13.2	1.392	74.6	16.4	10.6	0.634	31.2	32.6	13.4	1.926
Metric3D [14]	—	26.8	—	1.429	—	14.4	—	0.646	—	34.2	—	2.965
UniDepth-C [10]	62.8	23.8	11.5	0.968	81.1	14.8	8.30	0.536	43.3	35.5	10.3	1.532
UniDepth-V [10]	79.8	18.1	10.4	0.760	23.4	35.7	6.87	1.063	27.2	43.1	8.93	1.950
MfH (Ours)	42.2	34.5	13.2	1.363	67.7	23.3	9.73	0.738	47.1	24.0	8.16	1.366

Table 3: Ablation study for MRDE models and optimization targets on the NYUv2 dataset. True depth/disparity represents the performance with oracle depths/disparities as optimization targets.

MRDE Model	Optim. Target	$\delta_1 \uparrow$	AbsRel \downarrow	SI _{log} \downarrow	RMSE \downarrow
ZoeDepth [12]	true depth	63.9	22.4	24.5	0.692
	true disparity	66.5	20.1	23.2	0.658
	painted depth	29.5	35.5	30.6	1.246
	painted disparity	30.2	32.3	25.1	1.158
Marigold [1]	true depth	96.3	5.88	8.70	0.251
	true disparity	78.8	15.1	20.9	0.523
	painted depth	60.7	21.4	19.5	0.689
	painted disparity	40.7	31.1	31.3	1.086
Depth Anything [2]	true depth	75.8	16.8	19.8	0.657
	true disparity	97.9	4.57	6.68	0.222
	painted depth	50.1	41.7	27.9	1.874
	painted disparity	66.8	21.9	15.2	0.792

Table 4: Ablation study for optimization parameters and optimization targets on NYUv2. We optimize the predictions in the same space as optimization targets, i.e., the depth space for depth targets and the inverted depth space for disparity targets. The same applies to Tab. 3

Optim. Param.	Optim. Target	$\delta_1 \uparrow$	AbsRel \downarrow	SI _{log} \downarrow	RMSE \downarrow
s, t	true disparity	97.9	4.57	6.68	0.222
	painted disparity	58.6	28.0	21.2	1.079
$\{s_n\}, \{t_n\}, s$	true disparity	29.2	43.5	47.3	1.910
	painted disparity	29.6	74.4	36.6	3.000
$\{s_n\}, \{t_n\}, t$	true disparity	0.00	98.9	62.5	2.825
	painted disparity	0.30	113	182	3.387
$\{s_n\}, \{t_n\}, s, t$	true disparity	97.9	4.57	6.68	0.222
	painted disparity	66.8	21.9	15.2	0.792

In Tab. 2, we further provide a comparison between MfH and state-of-the-art many-shot methods, which are typically trained upon large-scale datasets with dense metric depth annotations. Our model achieves performance on par with, and sometimes superior to, these approaches, especially on ETH3D [54], which contains both indoor and outdoor scenes. It is noteworthy that these prior arts can do well on certain datasets while failing on others. For instance, ZeroDepth [11] performs well on iBims-1 but struggles to estimate depths on DIODE (Indoor) and ETH3D accurately. Similarly, UniDepth-V [10] shows promising results on DIODE (Indoor) while underperforming on the other two benchmarks. These findings signify the scene-dependent nature of existing fully supervised methods, which may result in degraded performance on unseen scenes. In contrast, our model demonstrates robust zero-shot generalization capabilities across diverse scenes. We further highlight the comparison among our MfH and Depth Anything [2] fine-tuned on NYUv2 or KITTI (2nd-3rd rows). These methods adopt a common Depth Anything MRDE backbone while deploying different strategies for MMDE. The results demonstrate that our test-time adaptation strategy generally works better than domain-specific fine-tuning, without the need for training on metric depth annotations.

4.3 Ablation Study

Impact of MRDE models. In Tab. 3, we investigate the performance of MfH with different MRDE models and various optimization targets. For ZoeDepth [12] and Depth Anything [2], we only adopt their pre-trained MRDE backbone as our MRDE model. Note that we use ground truth depths or disparities as optimization targets to show an approximate upper bound of performances, while only accessing painted depths or disparities as pseudo ground truths during real test-time adaptation. We also ensure consistency by optimizing predictions in the same space as the target, i.e., the depth space for depth targets and the inverted depth space for disparity targets. Overall, we observe using Depth Anything as our MRDE model and painted disparities as our optimization target shows the best performance. Comparing the first two rows and the last two rows for each MRDE model, we see that optimizations in the disparity space yield superior results for ZoeDepth [12] and Depth Anything [2], whereas optimizations in the depth space prove more effective for Marigold [1]. A similar scenario can also be found in the last two rows of each MRDE model. This variation in performance may stem from the difference in their output spaces. To be concrete, ZoeDepth and Depth Anything produce inverted depths, while Marigold outputs depths. Optimizing in the original output space can provide better numerical stability, leading to better optimization results.

Table 5: Ablation study for loss functions on NYUv2.

Loss	$\delta_1 \uparrow$	AbsRel \downarrow	SI _{log} \downarrow	RMSE \downarrow
l_1	24.2	201	28.9	4.645
l_2	62.3	27.1	16.7	0.975
MSE _{log}	67.5	22.5	14.6	0.810
SI _{log}	66.8	21.9	15.2	0.792

Figure 5: **Ablation study for the number of painted images on NYUv2.** Horizontal axis: $N \in \{4, 8, 16, 32\}$ inpainted images.

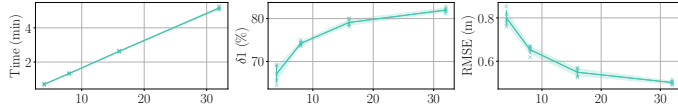


Figure 6: **An alternative perspective on MfH.** (a) Using camera intrinsics, the estimated metric depths can be transformed into a metric point cloud. (b) Our generate-and-estimate process can be seen as aligning the estimated point cloud of each painted human to its corresponding human mesh.

Impact of optimization parameters. In Tab. 4, we verify the benefits of aligning relative depth estimations of the original input and painted images with $\{s_n\}, \{t_n\}$ and parameterizing the metric head with s, t . We view the results from bottom to top. First, optimizing all parameters (7th-8th rows) yields the lowest error. When we fix the scaling factor to 1 while keeping the other parameters optimizable (5th-6th rows), the model has the highest error and cannot be aligned with the ground truth. Instead, when using optimizable scales (3rd-4th rows) in the metric head, the model can better capture depths, which indicates an accurate scene scale is crucial in MMDE. Removing the alignment between the input image MRDE and painted image MRDEs (1st-2nd rows) results in sub-optimal predictions since the same contents on two different images might result in distinct MRDE predictions. The performance difference of using different optimization parameters while the true disparity as the target (3rd vs. 5th vs. 7th row) shows it is possible to apply an affine transformation upon MRDE to achieve good MMDE predictions, if with accurate scale and translation recovered.

Impact of loss functions. In Tab. 5, we ablate the effect of using various loss functions for test-time training the metric head. Notably, employing an l_1 loss (1st row) yields inferior performance compared to losses incorporating an l_2 term (2nd-4th rows). This is probably because our generate-and-estimate process can introduce noises to a certain degree. Since the l_1 loss treats all errors equally, regardless of their magnitude, it can be more sensitive to small perturbations. An l_2 term that focuses more on large errors thus provides better robustness. Furthermore, a comparison between the 2nd and the last two rows shows optimizing in the log space brings better performance, which is expected since logarithmic transformation tends to mitigate the impact of outliers. This also accords with the general experience in training depth models using ground truth annotations, suggesting that the depths of generated humans might also be normally distributed in the log space, akin to real-world scenarios. From the last two rows, we see optimizing with the MSE_{log} loss or the SI_{log} loss is not discrepant by much. We opt for the SI_{log} loss in our optimization process due to its relatively superior AbsRel.

Impact of painting numbers N . In Fig. 5, we analyze the effect of increasing the number of painted images with humans. Specifically, we paint 4, 8, 16, and 32 images with humans, plotting curves as well as error bars for various metrics against the painting numbers. To draw reliable conclusions, we conduct experiments across five consistent random seeds for each painted image quantity. Our analysis reveals a clear linear association between the per-sample runtime and the number of painted images, as depicted in the time plot. The δ_1 and RMSE plots show an upward trend in MMDE performance with the increment in painting numbers, albeit sublinearly. By further examining the error bars, we see a larger number of painted images results in better robustness of predictions, which is demonstrated by a smaller, gradually converging standard deviation.

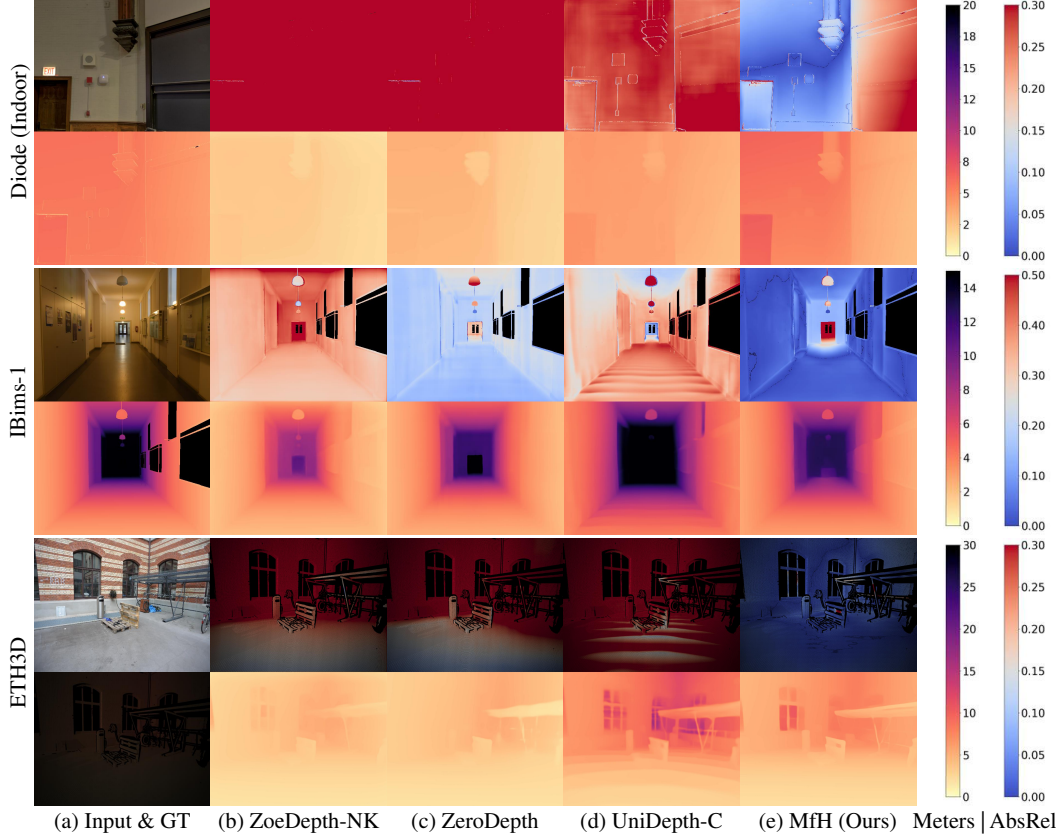


Figure 7: **Zero-shot qualitative results.** Each pair of consecutive rows corresponds to one test sample. Each odd row shows an input RGB image alongside the absolute relative error map, while each even row shows the ground truth metric depth and predicted metric depths.

4.4 Qualitative Analysis

We present an alternative view of our MfH in Fig. 6. With camera intrinsics, the estimated metric depths for both the painted images $\{\hat{D}_n^m\}$ and the original input D^m correspond to metric point clouds. Our MfH stretches the point clouds for $\{\hat{D}_n^m\}$ along the z-axis by setting human landmarks in 3D, revealing the 3D structure of the unpainted background in *meters*. With random painting, we progressively capture the 3D structure of the entire original input, thus bridging MRDE to MMDE.

We demonstrate metric depth predictions and pixel-wise AbsRel in Fig. 7, highlighting the strong zero-shot generalization ability of our MfH. Additionally, we show MMDE results for in-the-wild samples captured by DSLR cameras and smartphones in Fig. 8. Besides the robust performance of MfH, we observe that fully supervised MMDE methods like UniDepth [10] often provide bounded metric depths, inheriting from the limited range of sensors used in their training ground truths. In contrast, our MfH can provide more flexible results.

Case studies, user studies, and more qualitative analysis can be found in Appendix D.

5 Conclusion

We present MfH, a method that infers metric depths from in-the-wild images without the need for training on metric depth annotations. Utilizing humans as landmarks to extract metric scale priors from generative painting models, our approach addresses the challenge of scene dependency inherent in MMDE trained with metric depth supervision. Through a test-time adaptation pipeline, MfH effectively captures metric scale information from images by generating and estimating humans, which is then leveraged for zero-shot MMDE. Our experiments demonstrate that MfH achieves superior performance and better generalization ability compared to existing methods.

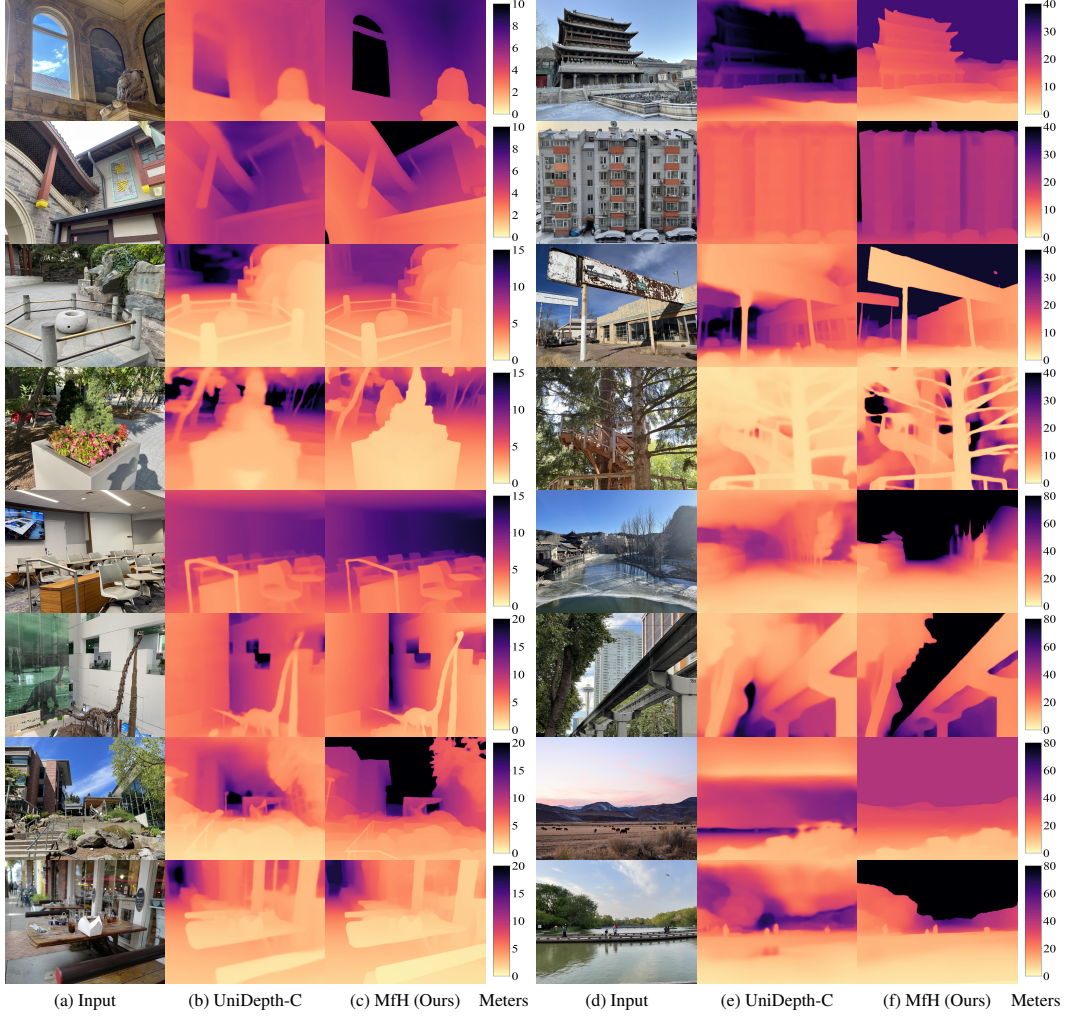


Figure 8: **In-the-wild qualitative results.** Each group of rows (a)-(c) or (d)-(f) corresponds to one in-the-wild test sample captured by a DSLR camera or a smartphone.

Limitation discussion. Our MfH works based on the assumption that humans can exist in the scene so that it is possible to paint a human upon the input image. While this holds for most usages of MMDE, it might not be ideal for some cases, e.g., close-up scenes. This opens up new challenges, such as incorporating objects other than humans into the generate-and-estimate pipeline as metric landmarks. Another assumption is the MRDE predictions align with true depths up to affine. Despite the training objectives of MRDE being linearly transformed true depths, the MRDE predictions can contain noises, making the linear metric head hard to capture accurate metric depths. Whether other parameterizations of the metric head can tackle this remains an open question.

Broader impacts. Our MfH decreases the demand for metric depth annotation which commonly requires depth sensors or stereo systems, making MMDE models more environmentally friendly. However, its usage of human-related models can perpetuate biases present in the training data, leading to unfair or discriminatory outcomes.

Acknowledgments and Disclosure of Funding

This study was partially funded by U.S. NIH grants R01GM134020 and P41GM103712, NSF grants DBI-1949629, DBI-2238093, IIS-2007595, IIS-2211597, and MCB-2205148. Additionally, it received support from Oracle Cloud credits and resources provided by Oracle for Research, as well as computational resources from the AMD HPC Fund.

References

- [1] Bingxin Ke, Anton Obukhov, Shengyu Huang, Nando Metzger, Rodrigo Caye Daudt, and Konrad Schindler. Repurposing diffusion-based image generators for monocular depth estimation. In *Proceedings of the IEEE/CVF Conference on Computer Vision and Pattern Recognition (CVPR)*, 2024.
- [2] Lihe Yang, Bingyi Kang, Zilong Huang, Xiaogang Xu, Jiashi Feng, and Hengshuang Zhao. Depth anything: Unleashing the power of large-scale unlabeled data. In *IEEE Conference on Computer Vision and Pattern Recognition (CVPR)*, 2024.
- [3] Xingshuai Dong, Matthew A Garratt, Sreenatha G Anavatti, and Hussein A Abbass. Towards real-time monocular depth estimation for robotics: A survey. *IEEE Transactions on Intelligent Transportation Systems*, 23(10):16940–16961, 2022.
- [4] Diana Wofk, Fangchang Ma, Tien-Ju Yang, Sertac Karaman, and Vivienne Sze. Fastdepth: Fast monocular depth estimation on embedded systems. In *2019 International Conference on Robotics and Automation (ICRA)*, pages 6101–6108. IEEE, 2019.
- [5] Dennis Park, Rares Ambrus, Vitor Guizilini, Jie Li, and Adrien Gaidon. Is pseudo-lidar needed for monocular 3d object detection? In *Proceedings of the IEEE/CVF International Conference on Computer Vision*, pages 3142–3152, 2021.
- [6] Wanli Peng, Hao Pan, He Liu, and Yi Sun. Ida-3d: Instance-depth-aware 3d object detection from stereo vision for autonomous driving. In *Proceedings of the IEEE/CVF Conference on Computer Vision and Pattern Recognition*, pages 13015–13024, 2020.
- [7] J Adam Jones, J Edward Swan, Gurjot Singh, Eric Kolstad, and Stephen R Ellis. The effects of virtual reality, augmented reality, and motion parallax on egocentric depth perception. In *Proceedings of the 5th symposium on Applied perception in graphics and visualization*, pages 9–14, 2008.
- [8] Fatima El Jamiy and Ronald Marsh. Survey on depth perception in head mounted displays: distance estimation in virtual reality, augmented reality, and mixed reality. *IET Image Processing*, 13(5):707–712, 2019.
- [9] René Ranftl, Katrin Lasinger, David Hafner, Konrad Schindler, and Vladlen Koltun. Towards robust monocular depth estimation: Mixing datasets for zero-shot cross-dataset transfer. *IEEE transactions on pattern analysis and machine intelligence*, 44(3):1623–1637, 2020.
- [10] Luigi Piccinelli, Yung-Hsu Yang, Christos Sakaridis, Mattia Segu, Siyuan Li, Luc Van Gool, and Fisher Yu. Unidepth: Universal monocular metric depth estimation. In *IEEE Conference on Computer Vision and Pattern Recognition (CVPR)*, 2024.
- [11] Vitor Guizilini, Igor Vasiljevic, Dian Chen, Rareş Ambruş, and Adrien Gaidon. Towards zero-shot scale-aware monocular depth estimation. In *Proceedings of the IEEE/CVF International Conference on Computer Vision*, pages 9233–9243, 2023.
- [12] Shariq Farooq Bhat, Reiner Birk, Diana Wofk, Peter Wonka, and Matthias Müller. Zoedepth: Zero-shot transfer by combining relative and metric depth. *arXiv preprint arXiv:2302.12288*, 2023.
- [13] Luigi Piccinelli, Christos Sakaridis, and Fisher Yu. idisc: Internal discretization for monocular depth estimation. In *Proceedings of the IEEE/CVF Conference on Computer Vision and Pattern Recognition*, pages 21477–21487, 2023.
- [14] Wei Yin, Chi Zhang, Hao Chen, Zhipeng Cai, Gang Yu, Kaixuan Wang, Xiaozhi Chen, and Chunhua Shen. Metric3d: Towards zero-shot metric 3d prediction from a single image. In *Proceedings of the IEEE/CVF International Conference on Computer Vision*, pages 9043–9053, 2023.
- [15] Weihao Yuan, Xiaodong Gu, Zuozhuo Dai, Siyu Zhu, and Ping Tan. Neural window fully-connected crfs for monocular depth estimation. In *Proceedings of the IEEE/CVF Conference on Computer Vision and Pattern Recognition*, pages 3916–3925, 2022.
- [16] Shariq Farooq Bhat, Ibraheem Alhashim, and Peter Wonka. Adabins: Depth estimation using adaptive bins. In *Proceedings of the IEEE/CVF conference on computer vision and pattern recognition*, pages 4009–4018, 2021.
- [17] Jin Han Lee, Myung-Kyu Han, Dong Wook Ko, and Il Hong Suh. From big to small: Multi-scale local planar guidance for monocular depth estimation. *arXiv preprint arXiv:1907.10326*, 2019.

[18] Maxime Oquab, Timothée Dariset, Théo Moutakanni, Huy Vo, Marc Szafraniec, Vasil Khalidov, Pierre Fernandez, Daniel Haziza, Francisco Massa, Alaeldin El-Nouby, et al. Dinov2: Learning robust visual features without supervision. *arXiv preprint arXiv:2304.07193*, 2023.

[19] Fabien Baradel, Matthieu Armando, Salma Galaaoui, Romain Brégier, Philippe Weinzaepfel, Grégory Rogez, and Thomas Lucas. Multi-hmr: Multi-person whole-body human mesh recovery in a single shot. *arXiv preprint arXiv:2402.14654*, 2024.

[20] Shubham Goel, Georgios Pavlakos, Jathushan Rajasegaran, Angjoo Kanazawa, and Jitendra Malik. Humans in 4d: Reconstructing and tracking humans with transformers. In *Proceedings of the IEEE/CVF International Conference on Computer Vision*, pages 14783–14794, 2023.

[21] Kevin Lin, Lijuan Wang, and Zicheng Liu. End-to-end human pose and mesh reconstruction with transformers. In *Proceedings of the IEEE/CVF conference on computer vision and pattern recognition*, pages 1954–1963, 2021.

[22] Matthew Loper, Naureen Mahmood, Javier Romero, Gerard Pons-Moll, and Michael J Black. Smpl: A skinned multi-person linear model. In *Seminal Graphics Papers: Pushing the Boundaries, Volume 2*, pages 851–866. 2023.

[23] Georgios Pavlakos, Vasileios Choutas, Nima Ghorbani, Timo Bolkart, Ahmed AA Osman, Dimitrios Tzionas, and Michael J Black. Expressive body capture: 3d hands, face, and body from a single image. In *Proceedings of the IEEE/CVF conference on computer vision and pattern recognition*, pages 10975–10985, 2019.

[24] Jinyoung Jun, Jae-Han Lee, Chul Lee, and Chang-Su Kim. Depth map decomposition for monocular depth estimation. In *European Conference on Computer Vision*, pages 18–34. Springer, 2022.

[25] Shariq Farooq Bhat, Ibraheem Alhashim, and Peter Wonka. Localbins: Improving depth estimation by learning local distributions. In *European Conference on Computer Vision*, pages 480–496. Springer, 2022.

[26] Zhenyu Li, Xuyang Wang, Xianming Liu, and Junjun Jiang. Binsformer: Revisiting adaptive bins for monocular depth estimation. *IEEE Transactions on Image Processing*, 2024.

[27] Alican Mertan, Damien Jade Duff, and Gozde Unal. Single image depth estimation: An overview. *Digital Signal Processing*, 123:103441, 2022.

[28] Jae-Han Lee and Chang-Su Kim. Monocular depth estimation using relative depth maps. In *Proceedings of the IEEE/CVF Conference on Computer Vision and Pattern Recognition*, pages 9729–9738, 2019.

[29] René Ranftl, Alexey Bochkovskiy, and Vladlen Koltun. Vision transformers for dense prediction. In *Proceedings of the IEEE/CVF International Conference on Computer Vision*, pages 12179–12188, 2021.

[30] Huan Fu, Mingming Gong, Chaohui Wang, Kayhan Batmanghelich, and Dacheng Tao. Deep ordinal regression network for monocular depth estimation. In *Proceedings of the IEEE Conference on Computer Vision and Pattern Recognition*, pages 2002–2011, 2018.

[31] Iro Laina, Christian Rupprecht, Vasileios Belagiannis, Federico Tombari, and Nassir Navab. Deeper depth prediction with fully convolutional residual networks. In *2016 Fourth international conference on 3D vision (3DV)*, pages 239–248. IEEE, 2016.

[32] Fayao Liu, Chunhua Shen, Guosheng Lin, and Ian Reid. Learning depth from single monocular images using deep convolutional neural fields. *IEEE transactions on pattern analysis and machine intelligence*, 38(10):2024–2039, 2015.

[33] Vaishakh Patil, Christos Sakaridis, Alexander Liniger, and Luc Van Gool. P3depth: Monocular depth estimation with a piecewise planarity prior. In *Proceedings of the IEEE/CVF Conference on Computer Vision and Pattern Recognition*, pages 1610–1621, 2022.

[34] Guanglei Yang, Hao Tang, Mingli Ding, Nicu Sebe, and Elisa Ricci. Transformer-based attention networks for continuous pixel-wise prediction. In *Proceedings of the IEEE/CVF International Conference on Computer vision*, pages 16269–16279, 2021.

[35] Ainaz Eftekhar, Alexander Sax, Jitendra Malik, and Amir Zamir. Omnidata: A scalable pipeline for making multi-task mid-level vision datasets from 3d scans. In *Proceedings of the IEEE/CVF International Conference on Computer Vision*, pages 10786–10796, 2021.

[36] Wei Yin, Jianming Zhang, Oliver Wang, Simon Niklaus, Long Mai, Simon Chen, and Chunhua Shen. Learning to recover 3d scene shape from a single image. In *Proceedings of the IEEE/CVF Conference on Computer Vision and Pattern Recognition*, pages 204–213, 2021.

[37] Jose M Facil, Benjamin Ummenhofer, Huizhong Zhou, Luis Montesano, Thomas Brox, and Javier Civera. Cam-convs: Camera-aware multi-scale convolutions for single-view depth. In *Proceedings of the IEEE/CVF Conference on Computer Vision and Pattern Recognition*, pages 11826–11835, 2019.

[38] Manuel López Antequera, Pau Gargallo, Markus Hofinger, Samuel Rota Bulò, Yubin Kuang, and Peter Kontschieder. Mapillary planet-scale depth dataset. In *Computer Vision–ECCV 2020: 16th European Conference, Glasgow, UK, August 23–28, 2020, Proceedings, Part II 16*, pages 589–604. Springer, 2020.

[39] Renrui Zhang, Ziyao Zeng, Ziyu Guo, and Yafeng Li. Can language understand depth? In *Proceedings of the 30th ACM International Conference on Multimedia*, pages 6868–6874, 2022.

[40] Xueting Hu, Ce Zhang, Yi Zhang, Bowen Hai, Ke Yu, and Zhihai He. Learning to adapt clip for few-shot monocular depth estimation. In *Proceedings of the IEEE/CVF Winter Conference on Applications of Computer Vision*, pages 5594–5603, 2024.

[41] Ziyao Zeng, Daniel Wang, Fengyu Yang, Hyoungseob Park, Stefano Soatto, Dong Lao, and Alex Wong. Wordepth: Variational language prior for monocular depth estimation. In *Proceedings of the IEEE/CVF Conference on Computer Vision and Pattern Recognition*, pages 9708–9719, 2024.

[42] Federica Bogo, Angjoo Kanazawa, Christoph Lassner, Peter Gehler, Javier Romero, and Michael J Black. Keep it smpl: Automatic estimation of 3d human pose and shape from a single image. In *Computer Vision–ECCV 2016: 14th European Conference, Amsterdam, The Netherlands, October 11–14, 2016, Proceedings, Part V 14*, pages 561–578. Springer, 2016.

[43] Garvita Tiwari, Dimitrije Antić, Jan Eric Lenssen, Nikolaos Sarafianos, Tony Tung, and Gerard Pons-Moll. Pose-ndf: Modeling human pose manifolds with neural distance fields. In *European Conference on Computer Vision*, pages 572–589. Springer, 2022.

[44] Angjoo Kanazawa, Michael J Black, David W Jacobs, and Jitendra Malik. End-to-end recovery of human shape and pose. In *Proceedings of the IEEE conference on Computer Vision and Pattern Recognition*, pages 7122–7131, 2018.

[45] Nikos Kolotouros, Georgios Pavlakos, Michael J Black, and Kostas Daniilidis. Learning to reconstruct 3d human pose and shape via model-fitting in the loop. In *Proceedings of the IEEE/CVF international conference on computer vision*, pages 2252–2261, 2019.

[46] Hongwen Zhang, Yating Tian, Xinchi Zhou, Wanli Ouyang, Yebin Liu, Limin Wang, and Zhenan Sun. Pymaf: 3d human pose and shape regression with pyramidal mesh alignment feedback loop. In *Proceedings of the IEEE/CVF International Conference on Computer Vision*, pages 11446–11456, 2021.

[47] Muhammed Kocabas, Chun-Hao P Huang, Otmar Hilliges, and Michael J Black. Pare: Part attention regressor for 3d human body estimation. In *Proceedings of the IEEE/CVF international conference on computer vision*, pages 11127–11137, 2021.

[48] Riza Alp Guler and Iasonas Kokkinos. Holopose: Holistic 3d human reconstruction in-the-wild. In *Proceedings of the IEEE/CVF conference on computer vision and pattern recognition*, pages 10884–10894, 2019.

[49] Yizhou Zhao, Tuanfeng Yang Wang, Bhiksha Raj, Min Xu, Jimei Yang, and Chun-Hao Paul Huang. Synergistic global-space camera and human reconstruction from videos. In *Proceedings of the IEEE/CVF Conference on Computer Vision and Pattern Recognition*, pages 1216–1226, 2024.

[50] Kaiming He, Georgia Gkioxari, Piotr Dollár, and Ross Girshick. Mask r-cnn. In *Proceedings of the IEEE International Conference on Computer Vision*, pages 2961–2969, 2017.

[51] David Eigen, Christian Puhrsch, and Rob Fergus. Depth map prediction from a single image using a multi-scale deep network. *Advances in neural information processing systems*, 27, 2014.

[52] Nathan Silberman, Derek Hoiem, Pushmeet Kohli, and Rob Fergus. Indoor segmentation and support inference from rgbd images. In *Computer Vision–ECCV 2012: 12th European Conference on Computer Vision, Florence, Italy, October 7–13, 2012, Proceedings, Part V 12*, pages 746–760. Springer, 2012.

[53] Tobias Koch, Lukas Liebel, Marco Körner, and Friedrich Fraundorfer. Comparison of monocular depth estimation methods using geometrically relevant metrics on the ibims-1 dataset. *Computer Vision and Image Understanding*, 191:102877, 2020.

[54] Thomas Schops, Johannes L Schonberger, Silvano Galliani, Torsten Sattler, Konrad Schindler, Marc Pollefeys, and Andreas Geiger. A multi-view stereo benchmark with high-resolution images and multi-camera videos. In *Proceedings of the IEEE conference on computer vision and pattern recognition*, pages 3260–3269, 2017.

[55] Andreas Geiger, Philip Lenz, and Raquel Urtasun. Are we ready for autonomous driving? the kitti vision benchmark suite. In *2012 IEEE conference on computer vision and pattern recognition*, pages 3354–3361. IEEE, 2012.

[56] Ravi Garg, Vijay Kumar Bg, Gustavo Carneiro, and Ian Reid. Unsupervised cnn for single view depth estimation: Geometry to the rescue. In *Computer Vision–ECCV 2016: 14th European Conference, Amsterdam, The Netherlands, October 11–14, 2016, Proceedings, Part VIII 14*, pages 740–756. Springer, 2016.

[57] Robin Rombach, Andreas Blattmann, Dominik Lorenz, Patrick Esser, and Björn Ommer. High-resolution image synthesis with latent diffusion models. In *Proceedings of the IEEE/CVF Conference on Computer Vision and Pattern Recognition*, pages 10684–10695, 2022.

[58] Shuai Li, Jiaying Shi, Wenfeng Song, Aimin Hao, and Hong Qin. Few-shot learning for monocular depth estimation based on local object relationship. In *2019 IEEE 31st International Conference on Tools with Artificial Intelligence (ICTAI)*, pages 1221–1228. IEEE, 2019.

[59] Renrui Zhang, Ziyao Zeng, Ziyu Guo, and Yafeng Li. Can language understand depth? In *Proceedings of the 30th ACM International Conference on Multimedia*, pages 6868–6874, 2022.

[60] Igor Vasiljevic, Nick Kolkin, Shanyi Zhang, Ruotian Luo, Haochen Wang, Falcon Z Dai, Andrea F Daniele, Mohammadreza Mostajabi, Steven Basart, Matthew R Walter, et al. Diode: A dense indoor and outdoor depth dataset. *arXiv preprint arXiv:1908.00463*, 2019.

[61] Tobias Koch, Lukas Liebel, Friedrich Fraundorfer, and Marco Korner. Evaluation of cnn-based single-image depth estimation methods. In *Proceedings of the European Conference on Computer Vision (ECCV) Workshops*, pages 0–0, 2018.

[62] Jathushan Rajasegaran, Georgios Pavlakos, Angjoo Kanazawa, and Jitendra Malik. Tracking people by predicting 3d appearance, location and pose. In *Proceedings of the IEEE/CVF Conference on Computer Vision and Pattern Recognition*, pages 2740–2749, 2022.

[63] Sai Kumar Dwivedi, Yu Sun, Priyanka Patel, Yao Feng, and Michael J Black. Tokenhmr: Advancing human mesh recovery with a tokenized pose representation. In *Proceedings of the IEEE/CVF Conference on Computer Vision and Pattern Recognition*, pages 1323–1333, 2024.

[64] Mu Hu, Wei Yin, Chi Zhang, Zhipeng Cai, Xiaoxiao Long, Hao Chen, Kaixuan Wang, Gang Yu, Chunhua Shen, and Shaojie Shen. Metric3d v2: A versatile monocular geometric foundation model for zero-shot metric depth and surface normal estimation. *arXiv preprint arXiv:2404.15506*, 2024.

A Experiments on Scene Dependency

A.1 Similarity with Training Samples

We provide more details of plotting MMDE δ_1 against the maximum cosine similarity between each test sample and all training samples in Fig. 3. Specifically, we run *ZoeDepth* [12] on each sample of its test sets and calculate their δ_1 metrics. We also calculate the cosine similarity of each test sample against each training sample with metric annotations with *DINOv2* [18] and find the similarity value for the nearest neighbor. Since *ZoeDepth* first pre-trains its backbone for MRDE and then finetunes on *NYUv2* [52] and *KITTI* [55] for MMDE, we only include the two datasets used for MMDE training during similarity calculation. For the scatter plot, we randomly take 10 different samples each time and plot their average δ_1 and maximum cosine similarity with training samples as one point on the figure. In this way, we plot 100 points for each testing dataset.

A.2 MRDE Performances of MMDE Models

Table 6: Performance comparisons of our MMDE methods in terms of MMDE and MRDE settings on the DIODE (Indoor) [60], iBims-1 [61], and ETH3D [54] datasets. *-{N, K, NK}: fine-tuned on *NYUv2* [52], *KITTI* [55], or the union of them. We re-evaluate all results with a fair and consistent pipeline for metric completeness.

Method	Setting	DIODE (Indoor)			iBims-1			ETH3D		
		$\delta_1 \uparrow$	AbsRel \downarrow	SI _{log} \downarrow	$\delta_1 \uparrow$	AbsRel \downarrow	SI _{log} \downarrow	$\delta_1 \uparrow$	AbsRel \downarrow	SI _{log} \downarrow
ZoeDepth-NK [12]	MMDE	38.8	33.0	13.3	61.0	18.7	8.98	33.5	47.3	14.0
Depth Anything-N [2]		29.7	32.7	12.5	71.3	15.0	7.58	25.2	38.7	10.2
Depth Anything-K [2]		11.1	231	15.5	2.88	217	17.2	16.9	136	17.1
ZeroDepth [11]		43.2	30.0	13.2	74.6	16.4	10.6	31.2	32.6	13.4
Metric3D [14]		—	26.8	—	—	14.4	—	—	34.2	—
UniDepth-C [10]		62.8	23.8	11.5	81.1	14.8	8.30	43.3	35.5	10.3
UniDepth-V [10]		79.8	18.1	10.4	23.4	35.7	6.87	27.2	43.1	8.93
ZoeDepth-NK [12]	MRDE	91.6	12.2	11.9	97.3	5.61	7.74	94.9	8.15	9.85
Depth Anything-N [2]		94.4	10.2	10.6	98.4	4.45	6.18	93.8	8.03	9.95
Depth Anything-K [2]		92.4	11.9	12.0	95.7	6.82	9.36	97.7	6.09	7.36
ZeroDepth [11]		91.8	12.1	12.1	94.8	6.51	9.25	87.6	11.6	12.1
UniDepth-C [10]		94.2	10.2	10.7	97.6	4.68	7.24	96.6	6.96	8.76
UniDepth-V [10]		95.6	8.89	9.78	98.6	3.41	5.69	97.4	5.79	7.53

To use an MMDE model for MRDE, we align the predictions with ground truths by solving optimal scales and translations. As demonstrated in Tab. 6, under the MRDE setting, MMDE models all perform well on in-the-wild data. In contrast, under the MMDE setting, they degrade to various degrees. These results show that, with fully supervised training, depth models are generally more generalizable under the MRDE setting than the MMDE setting. Since the MMDE task can be understood as a combination of MRDE and metric scale recovery, we believe the latter can be more difficult to conduct in the wild. Either implicitly or explicitly, conventional MMDE models predict metric scales in a discriminative manner, conditioned on the input image. With the fully supervised training scheme, they may tend to rely on the relation between training scenes and the testing scene to infer the metric scale. If the testing scene is unseen during training, it can be difficult to infer a scene scale. The MRDE task is relatively easier since it can potentially utilize more local visual clues for lower-level predictions. While establishing a global correspondence between training scenes and the testing scene might be challenging, the model can still identify local correspondences to predict relationships within different parts of a scene.

B More Ablation Study and Analysis

Impact of mask prompts. For generative painting, we randomly create mask prompts with heights h equal to the input image height H and widths $w \in [\alpha \cdot \min(H, W), \beta \cdot \min(H, W)]$, where $0 < \alpha < \beta < 1$ are two hyperparameters. In Tab. 7, we ablate the choices of them by painting $N = 4$ images with humans for each input. The results demonstrate that different α, β values will affect the model performance, while to a small degree. By comparing among the last three rows, we see the model performs better with smaller mask prompts within a reasonable range. When mask prompts

Table 7: Ablation study for mask sizes on the NYUv2 dataset.

Min Ratio α	Max Ratio β	$\delta_1 \uparrow$	AbsRel \downarrow	SI _{log} \downarrow	RMSE \downarrow
0.1	0.7	67.1	23.3	15.4	0.812
0.2	0.8	66.8	21.9	15.2	0.792
0.3	0.9	66.0	23.5	15.0	0.834
0.2	0.6	66.0	22.4	14.7	0.827
0.3	0.7	67.5	22.9	14.9	0.806
0.4	0.8	54.3	27.3	16.9	1.031

are constrained to larger sizes, as seen in the last row, model performance degrades. Moreover, when comparing rows (1st vs. 4th, 2nd vs. 5th, 3rd vs. 6th) with common centers $(\alpha + \beta)/2$ while different ranges $(\beta - \alpha)$, we observe larger ranges yields lower RMSE. This might be due to a larger range of mask sizes providing an opportunity to paint humans of more flexible sizes. As we can imagine, a close human will occupy larger areas in the painted image, and vice versa. This diversity leads to better numerical stabilities during solving the scale s and the translation t in Eq. (1). Therefore, we use $\alpha = 0.2, \beta = 0.8$ in our main experiments for optimal AbsRel results.

Table 8: Ablation study for different generative painting models on the NYUv2 dataset.

Model	$\delta_1 \uparrow$	AbsRel \downarrow	SI _{log} \downarrow	RMSE \downarrow
Stable Diffusion [57] v1.5	74.0	16.8	11.5	0.642
Stable Diffusion [57] XL	78.5	15.9	11.3	0.533
Stable Diffusion [57] v2	83.2	13.7	9.78	0.487

Table 9: Ablation study for different HMR models on the NYUv2 dataset.

Model	$\delta_1 \uparrow$	AbsRel \downarrow	SI _{log} \downarrow	RMSE \downarrow
HMR [62]	82.0	14.2	9.83	0.489
TokenHMR [63]	80.4	14.9	9.55	0.495
HMR 2.0 [20]	83.2	13.7	9.78	0.487

Impact of generative painting models. In Tab. 8, we show the effect of using different generative painting models by generating $N = 32$ images for each input. The results indicate that current generative painting models generally work well with MfH in MMDE. MfH combined with Stable Diffusion v2 produces the best outcomes, likely due to its superior ability to generate realistic paintings. It is possible that if a generation model can better capture the real-world 2D image distributions, it has a better sense of scale, serving as a more effective source of metric scale priors. Hence, we anticipate further performance gain of MfH with more advanced generative painting models.

Impact of HMR models. In Tab. 9, we evaluate the impact of using different HMR models within MfH. Here we use $N = 32$ painted images for each input. Our findings indicate that the performance of our approach remains stable regardless of the HMR model used, suggesting that humans serve as effective universal landmarks for deriving metric scales from images. Furthermore, current HMR models reliably contribute to extracting metric scales for MMDE within the MfH framework.

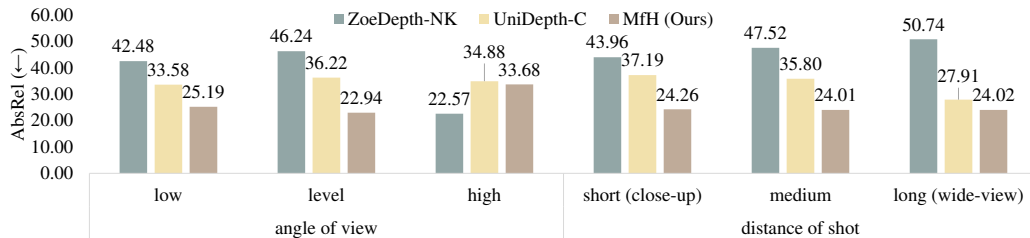


Figure 9: AbsRel (↓) comparisons for different types of shots on the ETH3D dataset.

Impact of input shot types. To analyze the contribution of metric information from humans, we look into the MMDE results on ETH3D [54], which includes both indoor and outdoor scenes with diverse shot types. Specifically, we annotate ETH3D images with two shot-related attributes and plot the AbsRel comparisons in Fig. 9. They confirm that our MfH can robustly recover metric depths, as it consistently achieves low errors across various types of shots. We also identify that the metric information from humans helps the most for level-angle inputs. This is likely because MRDE models

tend to interpret similar semantics, such as different parts of a human body, as having similar depths. This interpretation aligns well with standing humans, which are typically generated in level-angle images. Moreover, we do not observe significant degradation with varying the distance of shots. This indicates that MfH can effectively handle general close-up and wide-view shots.

C Difference with Previous Methods

Discriminative vs. Generative + Discriminative. Traditional MMDE models metric depth prediction in a discriminative manner. That is, given an input image I , they model a conditional probability of metric depths D^m with a neural network θ , i.e., $P_\theta(D^m|I)$. Further, the distribution of metric depths can be considered as a joint distribution of relative depths D^{rel} and metric scales S . According to the chain rule, we have

$$P_\theta(D^m|I) = P_\theta(D^{\text{rel}}, S|I) = P_\theta(D^{\text{rel}}|S, I) \cdot P_\theta(S|I). \quad (9)$$

Since the relative depth is scale-invariant, D^{rel} is independent to S ,

$$P_\theta(D^{\text{rel}}|S, I) = P_\theta(D^{\text{rel}}|I) \Rightarrow P_\theta(D^m|I) = P_\theta(D^{\text{rel}}|I) \cdot P_\theta(S|I). \quad (10)$$

Most prior arts [12, 11, 14, 10, 2] parameterize the two terms $p_\theta(D^{\text{rel}}|I), p_\theta(S|I)$ jointly with a single discriminative θ . In contrast, we consider introducing generative and discriminative priors in modeling $P(S|I)$. With the law of total probability, we have

$$P(S|I) = \sum_{I^{\text{paint}}} P(S|I^{\text{paint}}, I) \cdot P(I^{\text{paint}}|I), \quad (11)$$

where I^{paint} is the random variable for the painted image. In this equation, $P(I^{\text{paint}}|I)$ can be captured by the generative painting model conditioned on the input, and $P(S|I^{\text{paint}}, I)$ is estimated by HMR and our metric head, which are discriminative. The summation over I^{paint} corresponds to our global optimization upon random generative painting. Our MfH can thus approximate $P(S|I)$ through Monte Carlo sampling, bridging the gap between MRDE, i.e., $P(D^{\text{rel}}|I)$, and MMDE, i.e., $P(D^m|I)$.

Training vs. Pre-training + Fine-tuning vs. Test-time Adaptation Most traditional MMDE approaches [17, 16, 15, 13, 11, 14, 10] follow a fully supervised training paradigm, for which we discuss can cause dependency to training scenes during test time. For them, expensive metric depth annotations on diverse scenes are necessary for zero-shot abilities. Some recent works seek to reduce the cost of data labeling by introducing pretraining over relative depth [12] or unlabeled image data [2]. While this mitigates the data hunger to some degree, these works also require downstream fine-tuning with metric depth annotations for MMDE. We instead consider a test-time adaptation scenario having no access to metric annotations. Under this setting, our model is required to predict the metric depth merely dependent on one input image.

D More Qualitative Analysis

D.1 Case Study

Since the performance of MfH relies on the quality of the pseudo ground truths $\{\mathbf{D}_n^*\}$, we illustrate both successful and failed cases generated during this process in Fig. 10. Typical failure cases, shown in the first three rows, include 1) the generative painting model producing non-human objects with human features (1st row), 2) the generative painting model incorrectly capturing the scene scale and producing out-of-proportion humans (2nd row), and 3) the human mesh recovery model predicting meshes that penetrate each other (3rd row). In contrast, success cases in the last three rows demonstrate accurate space and scale relationships between human figures and scenes, leading to effective pseudo ground truths. These visualizations partially explain why more painted images help to improve the MMDE performance. The reason is that a larger number of painted images dilutes the influence of outliers, facilitating a more robust optimization. We hence speculate prompt engineering, as well as better sampling and filtering strategies in human painting, can further improve the performance of MfH. We leave the exploration of these to future work.



Figure 10: **Success cases and failure cases of MfH during the process of pseudo ground truth D_n^* generation.** The first three rows show failure cases, while the last three rows show success ones.

D.2 User Study

We further conduct a user study for in-the-wild inputs where ground truths are unavailable. This study includes MMDE results from DepthAnything- $\{N, K\}$ [2], Metric3D-v1 [14], Metric3D-v2 [64], UniDepth- $\{C, V\}$ [10], ZeroDepth [11], ZoeDepth-NK [12], and our proposed MfH. As shown in Fig. 11, participants are presented with input images, corresponding MMDE results from the above-listed methods, along with a color bar mapping metric depth values to colors. They were instructed to select the most reasonable MMDE result for each sample, with the following guidance:

Please choose the most reasonable metric depth estimation for each question given the input image and the meter bar. Different colors represent different metric depth values. Note that depth values farther than the maximum value or nearer than the minimum value on the meter bar are truncated.

To analyze the results, we take each input image as a separate sample and add one count to the corresponding method if its MMDE result is selected as the most reasonable MMDE given the corresponding input image and the meter bar. We then calculate the selection rate for each method, representing the proportion of selected results for this method out of the total number of selections. We received 50 responses with the results in Tab. 10. According to the meter bar attached, we roughly break down the selection rate for short, medium, and long depth ranges.

These results indicate that our MfH method achieves the highest selection rate across all depth ranges, demonstrating its robustness. Metric3D-v2 also performs well, securing the second-highest selection

Table 10: Selection rate as the most reasonable MMDE result across different ranges. The ranges indicate the maximum value of the meter bar related to each input sample.

Range	Max Depth	DA-K [2]	DA-N [2]	M3D-v1 [14]	M3D-v2 [64]	UD-C [10]	UD-V [10]	0D [11]	ZD-NK [12]	MfH (Ours)
Short-range	10m-15m	4.0%	14.4%	0.0%	18.8%	6.0%	12.8%	1.6%	3.6%	38.8%
Medium-range	20m-40m	17.7%	3.1%	2.0%	16.6%	6.0%	2.6%	0.3%	4.9%	46.9%
Long-range	80m	13.5%	2.0%	11.0%	21.0%	6.0%	2.5%	0.5%	3.5%	40.0%
Overall	10m-80m	12.4%	6.4%	3.6%	18.4%	6.0%	5.8%	0.8%	4.1%	42.6%

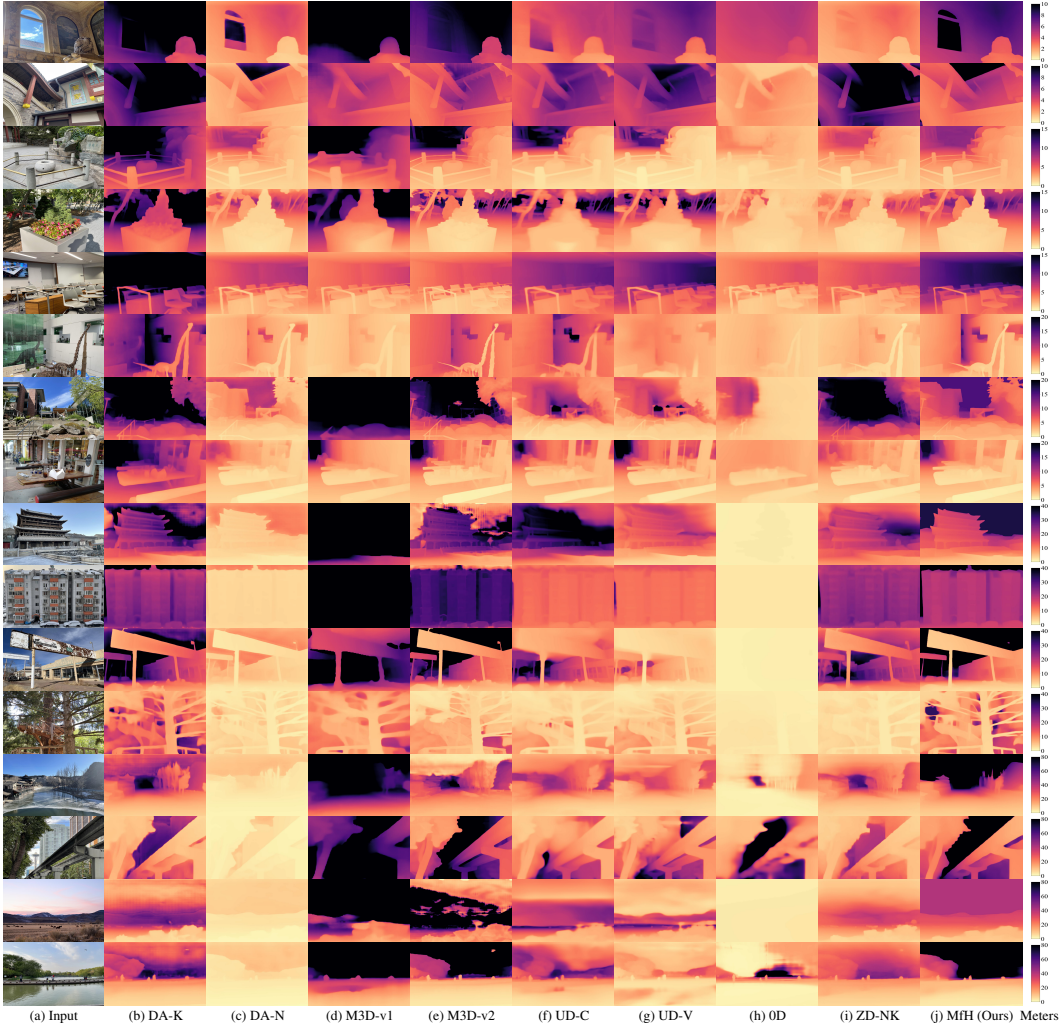


Figure 11: **In-the-wild qualitative results for DSLR camera or smartphone captured images.**

rate. In contrast, other methods show variability in performance across different depth ranges. For example, DepthAnything-N has a high selection rate for short-range inputs but is not selected for inputs with larger maximum depths. This is probably due to its scene dependency. Since it is trained on NYUv2, an indoor scene dataset, its MMDE ability focuses more on short-range scenes.

D.3 Zero-shot Qualitative Results

We demonstrate more metric depth predictions and pixel-wise AbsRel in Figs. 12 to 16.

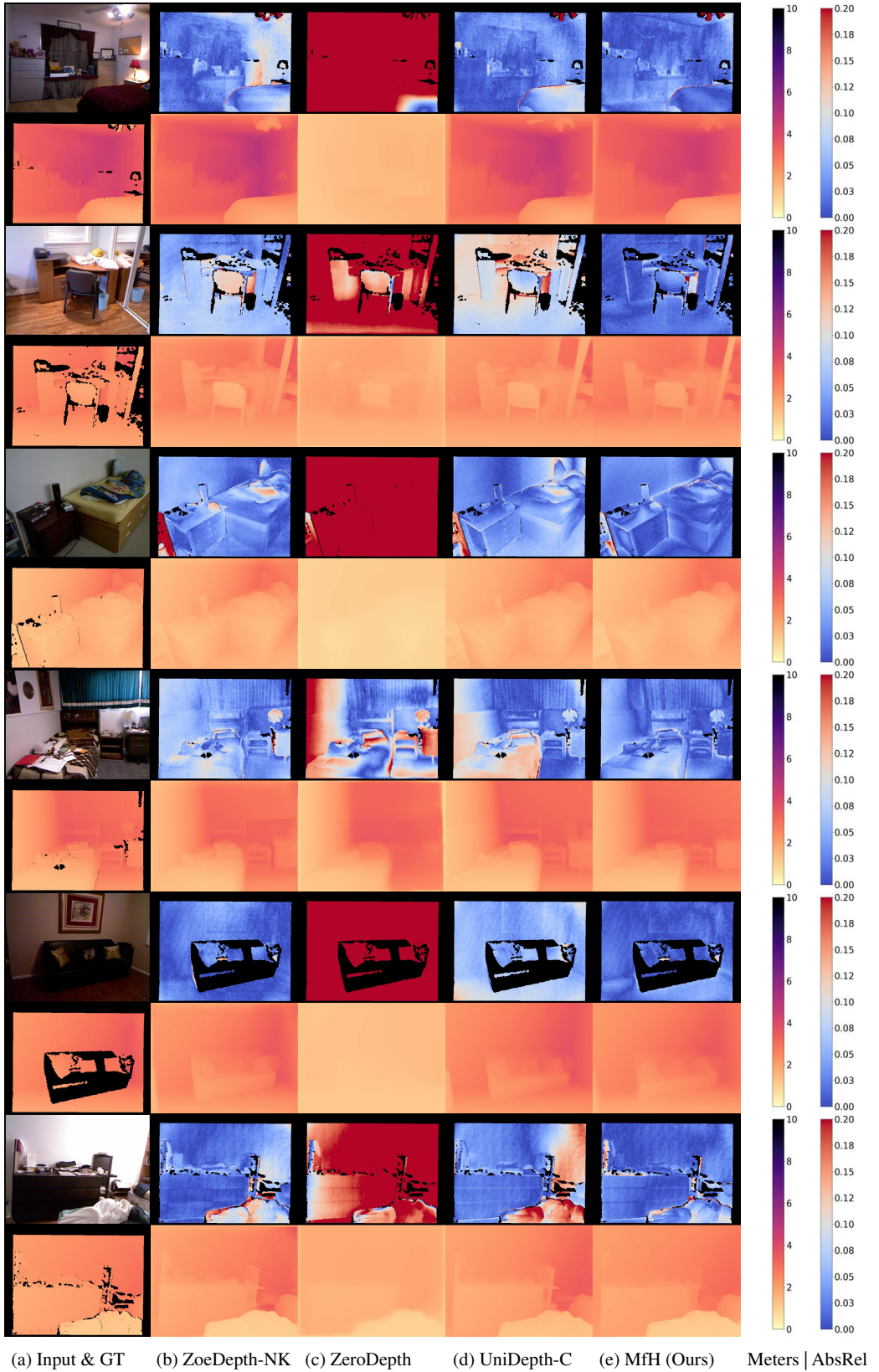


Figure 12: **Zero-shot qualitative results on NYU Depth v2.**

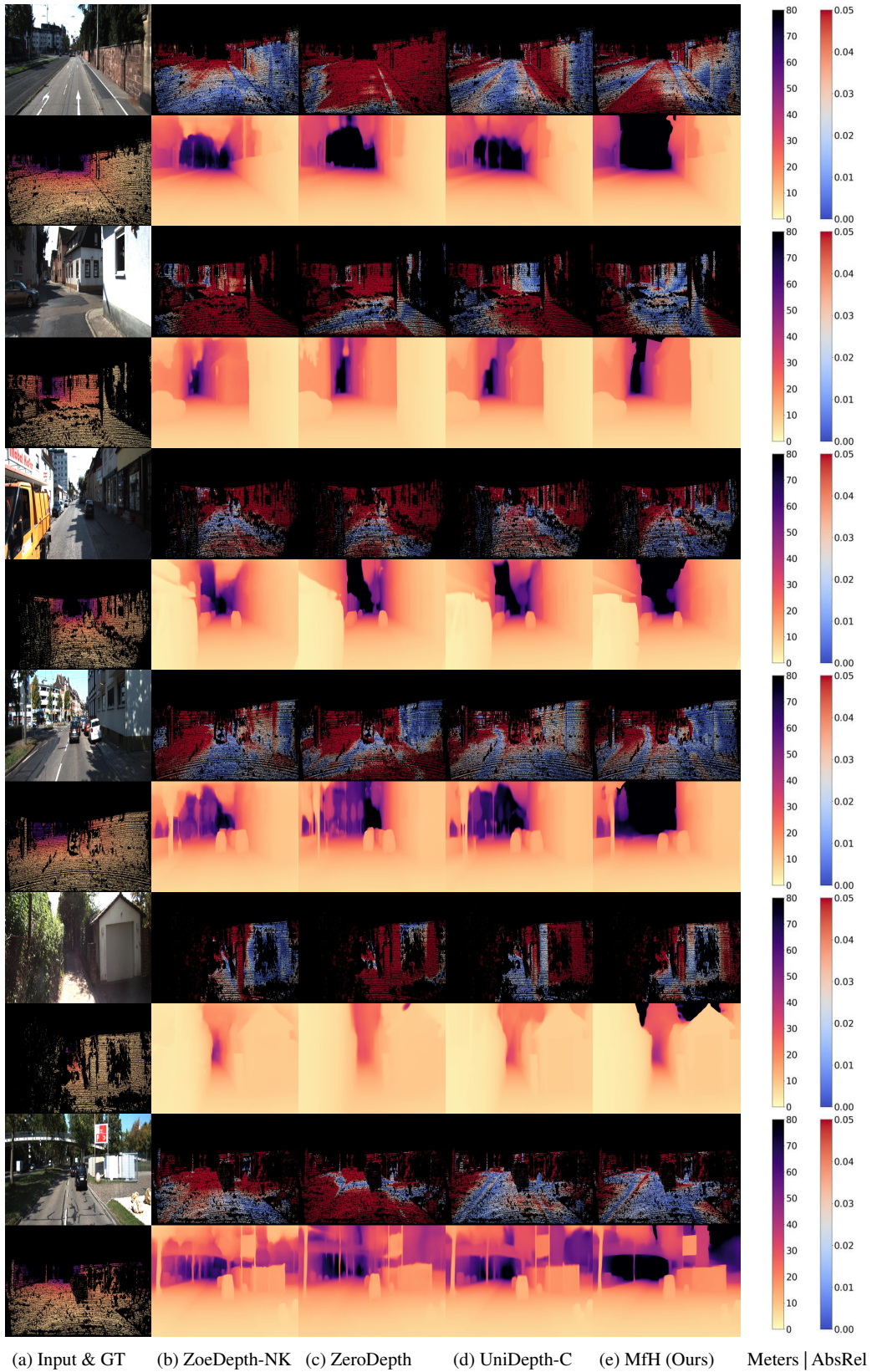


Figure 13: **Zero-shot qualitative results on KITTI.**

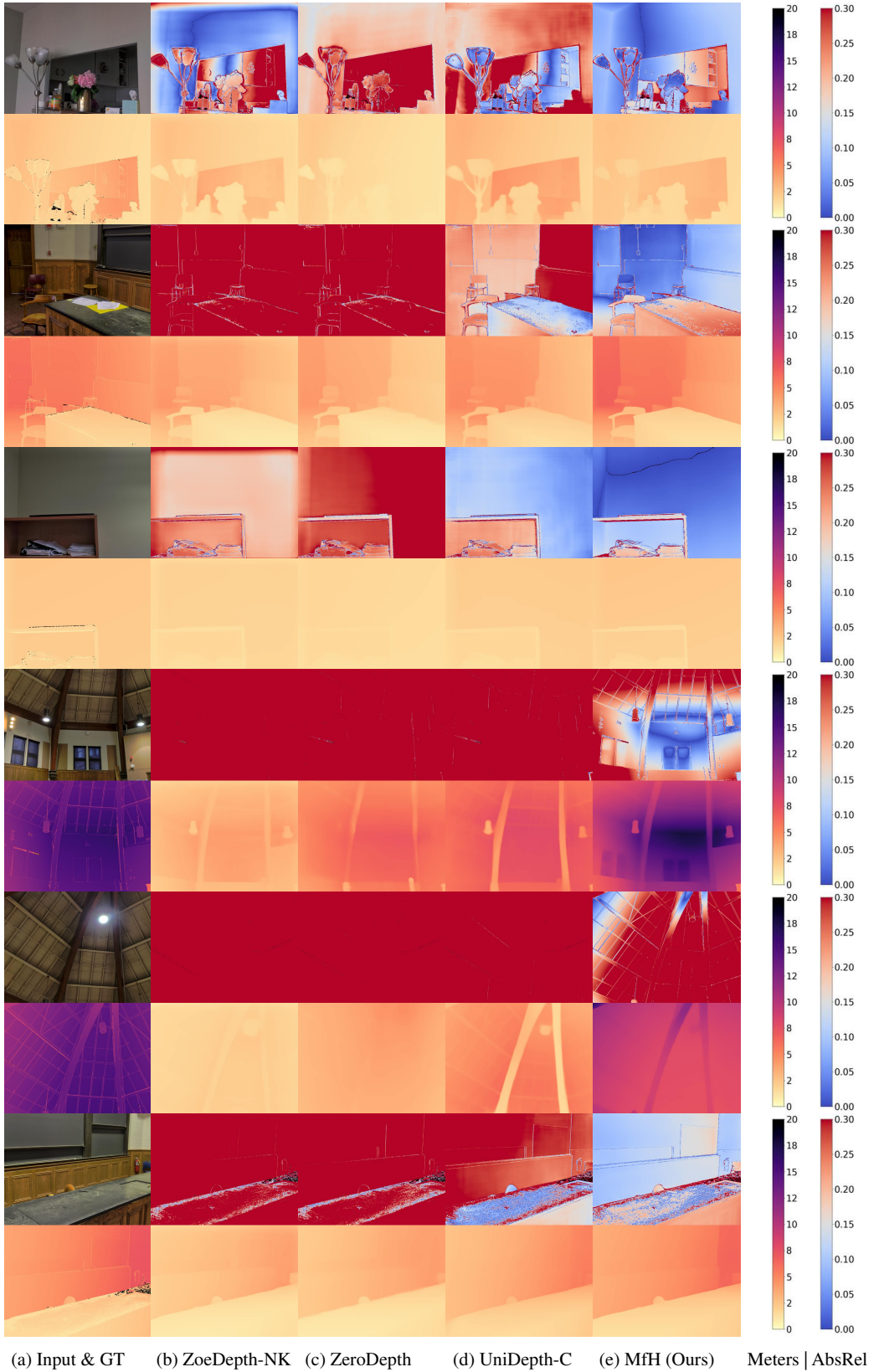


Figure 14: **Zero-shot qualitative results on Diode (Indoor).**

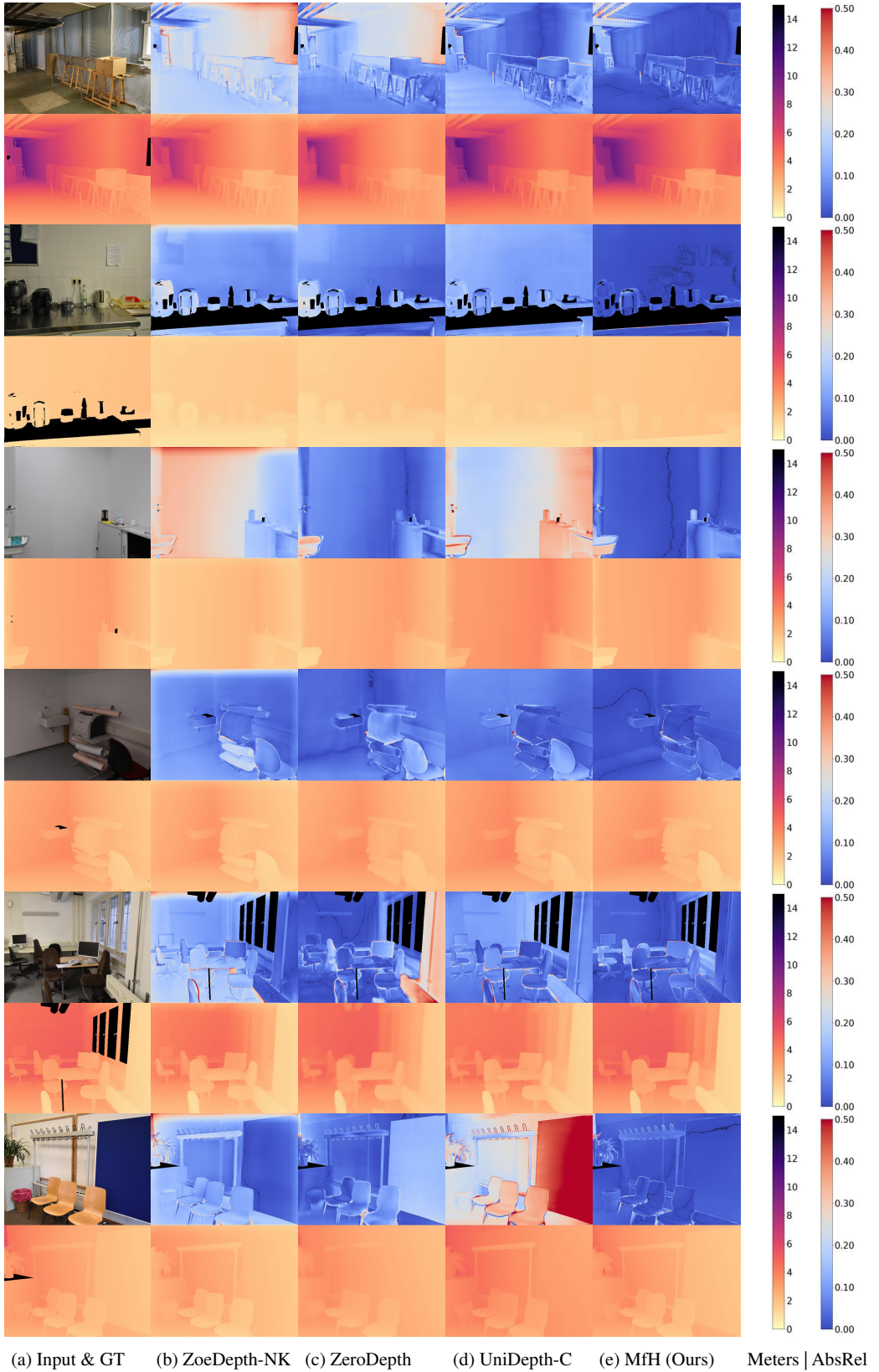


Figure 15: **Zero-shot qualitative results on iBims-1.**

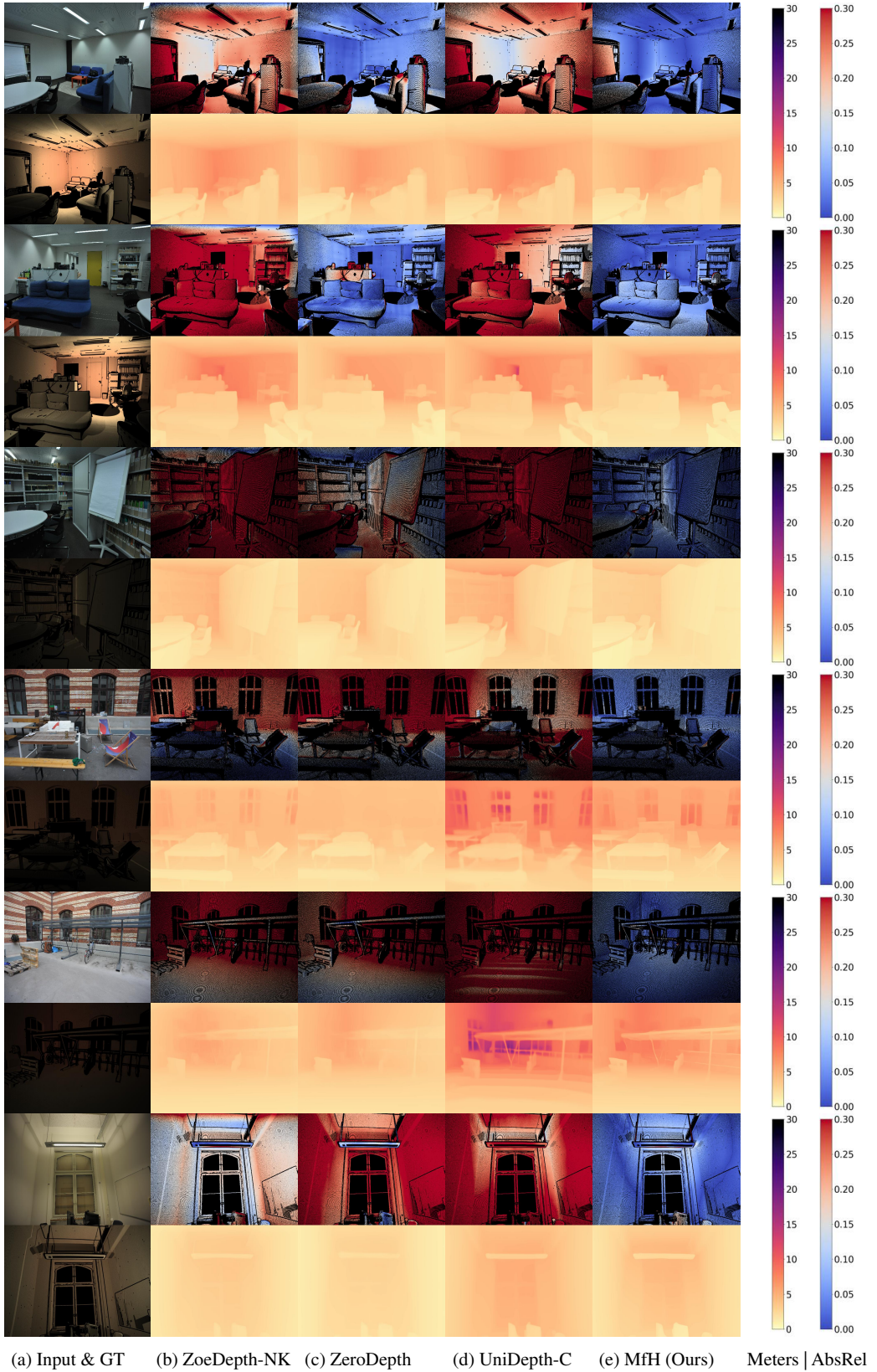


Figure 16: **Zero-shot qualitative results on ETH3D.**

NeurIPS Paper Checklist

1. Claims

Question: Do the main claims made in the abstract and introduction accurately reflect the paper's contributions and scope?

Answer: [\[Yes\]](#)

Justification: We discuss the paper's contributions and scope in Sec. 1.

Guidelines:

- The answer NA means that the abstract and introduction do not include the claims made in the paper.
- The abstract and/or introduction should clearly state the claims made, including the contributions made in the paper and important assumptions and limitations. A No or NA answer to this question will not be perceived well by the reviewers.
- The claims made should match theoretical and experimental results, and reflect how much the results can be expected to generalize to other settings.
- It is fine to include aspirational goals as motivation as long as it is clear that these goals are not attained by the paper.

2. Limitations

Question: Does the paper discuss the limitations of the work performed by the authors?

Answer: [\[Yes\]](#)

Justification: We discuss the limitations in Sec. 5.

Guidelines:

- The answer NA means that the paper has no limitation while the answer No means that the paper has limitations, but those are not discussed in the paper.
- The authors are encouraged to create a separate "Limitations" section in their paper.
- The paper should point out any strong assumptions and how robust the results are to violations of these assumptions (e.g., independence assumptions, noiseless settings, model well-specification, asymptotic approximations only holding locally). The authors should reflect on how these assumptions might be violated in practice and what the implications would be.
- The authors should reflect on the scope of the claims made, e.g., if the approach was only tested on a few datasets or with a few runs. In general, empirical results often depend on implicit assumptions, which should be articulated.
- The authors should reflect on the factors that influence the performance of the approach. For example, a facial recognition algorithm may perform poorly when image resolution is low or images are taken in low lighting. Or a speech-to-text system might not be used reliably to provide closed captions for online lectures because it fails to handle technical jargon.
- The authors should discuss the computational efficiency of the proposed algorithms and how they scale with dataset size.
- If applicable, the authors should discuss possible limitations of their approach to address problems of privacy and fairness.
- While the authors might fear that complete honesty about limitations might be used by reviewers as grounds for rejection, a worse outcome might be that reviewers discover limitations that aren't acknowledged in the paper. The authors should use their best judgment and recognize that individual actions in favor of transparency play an important role in developing norms that preserve the integrity of the community. Reviewers will be specifically instructed to not penalize honesty concerning limitations.

3. Theory Assumptions and Proofs

Question: For each theoretical result, does the paper provide the full set of assumptions and a complete (and correct) proof?

Answer: [\[NA\]](#)

Justification: There are no theoretical results in our paper.

Guidelines:

- The answer NA means that the paper does not include theoretical results.
- All the theorems, formulas, and proofs in the paper should be numbered and cross-referenced.
- All assumptions should be clearly stated or referenced in the statement of any theorems.
- The proofs can either appear in the main paper or the supplemental material, but if they appear in the supplemental material, the authors are encouraged to provide a short proof sketch to provide intuition.
- Inversely, any informal proof provided in the core of the paper should be complemented by formal proofs provided in appendix or supplemental material.
- Theorems and Lemmas that the proof relies upon should be properly referenced.

4. Experimental Result Reproducibility

Question: Does the paper fully disclose all the information needed to reproduce the main experimental results of the paper to the extent that it affects the main claims and/or conclusions of the paper (regardless of whether the code and data are provided or not)?

Answer: **[Yes]**

Justification: We provide detailed experimental settings for our main experiment in Sec. 4.1, and details of our pilot experiments in Appendix A.

Guidelines:

- The answer NA means that the paper does not include experiments.
- If the paper includes experiments, a No answer to this question will not be perceived well by the reviewers: Making the paper reproducible is important, regardless of whether the code and data are provided or not.
- If the contribution is a dataset and/or model, the authors should describe the steps taken to make their results reproducible or verifiable.
- Depending on the contribution, reproducibility can be accomplished in various ways. For example, if the contribution is a novel architecture, describing the architecture fully might suffice, or if the contribution is a specific model and empirical evaluation, it may be necessary to either make it possible for others to replicate the model with the same dataset, or provide access to the model. In general, releasing code and data is often one good way to accomplish this, but reproducibility can also be provided via detailed instructions for how to replicate the results, access to a hosted model (e.g., in the case of a large language model), releasing of a model checkpoint, or other means that are appropriate to the research performed.
- While NeurIPS does not require releasing code, the conference does require all submissions to provide some reasonable avenue for reproducibility, which may depend on the nature of the contribution. For example
 - (a) If the contribution is primarily a new algorithm, the paper should make it clear how to reproduce that algorithm.
 - (b) If the contribution is primarily a new model architecture, the paper should describe the architecture clearly and fully.
 - (c) If the contribution is a new model (e.g., a large language model), then there should either be a way to access this model for reproducing the results or a way to reproduce the model (e.g., with an open-source dataset or instructions for how to construct the dataset).
 - (d) We recognize that reproducibility may be tricky in some cases, in which case authors are welcome to describe the particular way they provide for reproducibility. In the case of closed-source models, it may be that access to the model is limited in some way (e.g., to registered users), but it should be possible for other researchers to have some path to reproducing or verifying the results.

5. Open access to data and code

Question: Does the paper provide open access to the data and code, with sufficient instructions to faithfully reproduce the main experimental results, as described in supplemental material?

Answer: [\[Yes\]](#)

Justification: Our code is available at <https://github.com/Skaldak/MfH>.

Guidelines:

- The answer NA means that paper does not include experiments requiring code.
- Please see the NeurIPS code and data submission guidelines (<https://nips.cc/public/guides/CodeSubmissionPolicy>) for more details.
- While we encourage the release of code and data, we understand that this might not be possible, so “No” is an acceptable answer. Papers cannot be rejected simply for not including code, unless this is central to the contribution (e.g., for a new open-source benchmark).
- The instructions should contain the exact command and environment needed to run to reproduce the results. See the NeurIPS code and data submission guidelines (<https://nips.cc/public/guides/CodeSubmissionPolicy>) for more details.
- The authors should provide instructions on data access and preparation, including how to access the raw data, preprocessed data, intermediate data, and generated data, etc.
- The authors should provide scripts to reproduce all experimental results for the new proposed method and baselines. If only a subset of experiments are reproducible, they should state which ones are omitted from the script and why.
- At submission time, to preserve anonymity, the authors should release anonymized versions (if applicable).
- Providing as much information as possible in supplemental material (appended to the paper) is recommended, but including URLs to data and code is permitted.

6. Experimental Setting/Details

Question: Does the paper specify all the training and test details (e.g., data splits, hyper-parameters, how they were chosen, type of optimizer, etc.) necessary to understand the results?

Answer: [\[Yes\]](#)

Justification: We provide detailed experimental settings for our main experiment in Sec. 4.1, and details of our pilot experiments in Appendix A.

Guidelines:

- The answer NA means that the paper does not include experiments.
- The experimental setting should be presented in the core of the paper to a level of detail that is necessary to appreciate the results and make sense of them.
- The full details can be provided either with the code, in appendix, or as supplemental material.

7. Experiment Statistical Significance

Question: Does the paper report error bars suitably and correctly defined or other appropriate information about the statistical significance of the experiments?

Answer: [\[Yes\]](#)

Justification: We plot the results with error bars in Fig. 5.

Guidelines:

- The answer NA means that the paper does not include experiments.
- The authors should answer “Yes” if the results are accompanied by error bars, confidence intervals, or statistical significance tests, at least for the experiments that support the main claims of the paper.
- The factors of variability that the error bars are capturing should be clearly stated (for example, train/test split, initialization, random drawing of some parameter, or overall run with given experimental conditions).
- The method for calculating the error bars should be explained (closed form formula, call to a library function, bootstrap, etc.)
- The assumptions made should be given (e.g., Normally distributed errors).

- It should be clear whether the error bar is the standard deviation or the standard error of the mean.
- It is OK to report 1-sigma error bars, but one should state it. The authors should preferably report a 2-sigma error bar than state that they have a 96% CI, if the hypothesis of Normality of errors is not verified.
- For asymmetric distributions, the authors should be careful not to show in tables or figures symmetric error bars that would yield results that are out of range (e.g. negative error rates).
- If error bars are reported in tables or plots, The authors should explain in the text how they were calculated and reference the corresponding figures or tables in the text.

8. Experiments Compute Resources

Question: For each experiment, does the paper provide sufficient information on the computer resources (type of compute workers, memory, time of execution) needed to reproduce the experiments?

Answer: [\[Yes\]](#)

Justification: We provide information on the computer resources in Sec. 4.1.

Guidelines:

- The answer NA means that the paper does not include experiments.
- The paper should indicate the type of compute workers CPU or GPU, internal cluster, or cloud provider, including relevant memory and storage.
- The paper should provide the amount of compute required for each of the individual experimental runs as well as estimate the total compute.
- The paper should disclose whether the full research project required more compute than the experiments reported in the paper (e.g., preliminary or failed experiments that didn't make it into the paper).

9. Code Of Ethics

Question: Does the research conducted in the paper conform, in every respect, with the NeurIPS Code of Ethics <https://neurips.cc/public/EthicsGuidelines>?

Answer: [\[Yes\]](#)

Justification: The paper conforms to the NeurIPS Code of Ethics.

Guidelines:

- The answer NA means that the authors have not reviewed the NeurIPS Code of Ethics.
- If the authors answer No, they should explain the special circumstances that require a deviation from the Code of Ethics.
- The authors should make sure to preserve anonymity (e.g., if there is a special consideration due to laws or regulations in their jurisdiction).

10. Broader Impacts

Question: Does the paper discuss both potential positive societal impacts and negative societal impacts of the work performed?

Answer: [\[Yes\]](#)

Justification: We discuss both positive societal impacts and negative societal impacts in Sec. 5.

Guidelines:

- The answer NA means that there is no societal impact of the work performed.
- If the authors answer NA or No, they should explain why their work has no societal impact or why the paper does not address societal impact.
- Examples of negative societal impacts include potential malicious or unintended uses (e.g., disinformation, generating fake profiles, surveillance), fairness considerations (e.g., deployment of technologies that could make decisions that unfairly impact specific groups), privacy considerations, and security considerations.

- The conference expects that many papers will be foundational research and not tied to particular applications, let alone deployments. However, if there is a direct path to any negative applications, the authors should point it out. For example, it is legitimate to point out that an improvement in the quality of generative models could be used to generate deepfakes for disinformation. On the other hand, it is not needed to point out that a generic algorithm for optimizing neural networks could enable people to train models that generate Deepfakes faster.
- The authors should consider possible harms that could arise when the technology is being used as intended and functioning correctly, harms that could arise when the technology is being used as intended but gives incorrect results, and harms following from (intentional or unintentional) misuse of the technology.
- If there are negative societal impacts, the authors could also discuss possible mitigation strategies (e.g., gated release of models, providing defenses in addition to attacks, mechanisms for monitoring misuse, mechanisms to monitor how a system learns from feedback over time, improving the efficiency and accessibility of ML).

11. Safeguards

Question: Does the paper describe safeguards that have been put in place for responsible release of data or models that have a high risk for misuse (e.g., pretrained language models, image generators, or scraped datasets)?

Answer: [NA]

Justification: This paper poses no such risks.

Guidelines:

- The answer NA means that the paper poses no such risks.
- Released models that have a high risk for misuse or dual-use should be released with necessary safeguards to allow for controlled use of the model, for example by requiring that users adhere to usage guidelines or restrictions to access the model or implementing safety filters.
- Datasets that have been scraped from the Internet could pose safety risks. The authors should describe how they avoided releasing unsafe images.
- We recognize that providing effective safeguards is challenging, and many papers do not require this, but we encourage authors to take this into account and make a best faith effort.

12. Licenses for existing assets

Question: Are the creators or original owners of assets (e.g., code, data, models), used in the paper, properly credited and are the license and terms of use explicitly mentioned and properly respected?

Answer: [Yes]

Justification: We cite all used public datasets and pre-trained models in Sec. 4.1.

Guidelines:

- The answer NA means that the paper does not use existing assets.
- The authors should cite the original paper that produced the code package or dataset.
- The authors should state which version of the asset is used and, if possible, include a URL.
- The name of the license (e.g., CC-BY 4.0) should be included for each asset.
- For scraped data from a particular source (e.g., website), the copyright and terms of service of that source should be provided.
- If assets are released, the license, copyright information, and terms of use in the package should be provided. For popular datasets, paperswithcode.com/datasets has curated licenses for some datasets. Their licensing guide can help determine the license of a dataset.
- For existing datasets that are re-packaged, both the original license and the license of the derived asset (if it has changed) should be provided.

- If this information is not available online, the authors are encouraged to reach out to the asset's creators.

13. New Assets

Question: Are new assets introduced in the paper well documented and is the documentation provided alongside the assets?

Answer: [NA]

Justification: We do not introduce new assets in the paper.

Guidelines:

- The answer NA means that the paper does not release new assets.
- Researchers should communicate the details of the dataset/code/model as part of their submissions via structured templates. This includes details about training, license, limitations, etc.
- The paper should discuss whether and how consent was obtained from people whose asset is used.
- At submission time, remember to anonymize your assets (if applicable). You can either create an anonymized URL or include an anonymized zip file.

14. Crowdsourcing and Research with Human Subjects

Question: For crowdsourcing experiments and research with human subjects, does the paper include the full text of instructions given to participants and screenshots, if applicable, as well as details about compensation (if any)?

Answer: [NA]

Justification: This paper does not involve crowdsourcing or research with human subjects.

Guidelines:

- The answer NA means that the paper does not involve crowdsourcing nor research with human subjects.
- Including this information in the supplemental material is fine, but if the main contribution of the paper involves human subjects, then as much detail as possible should be included in the main paper.
- According to the NeurIPS Code of Ethics, workers involved in data collection, curation, or other labor should be paid at least the minimum wage in the country of the data collector.

15. Institutional Review Board (IRB) Approvals or Equivalent for Research with Human Subjects

Question: Does the paper describe potential risks incurred by study participants, whether such risks were disclosed to the subjects, and whether Institutional Review Board (IRB) approvals (or an equivalent approval/review based on the requirements of your country or institution) were obtained?

Answer: [NA]

Justification: This paper does not involve research with human subjects.

Guidelines:

- The answer NA means that the paper does not involve crowdsourcing nor research with human subjects.
- Depending on the country in which research is conducted, IRB approval (or equivalent) may be required for any human subjects research. If you obtained IRB approval, you should clearly state this in the paper.
- We recognize that the procedures for this may vary significantly between institutions and locations, and we expect authors to adhere to the NeurIPS Code of Ethics and the guidelines for their institution.
- For initial submissions, do not include any information that would break anonymity (if applicable), such as the institution conducting the review.